Robust Design Optimization applied to Structural, Thermal and Fluid Analysis including Manufacturing Tolerances

Dirk Roos[1]*, Johannes Einzinger[2] & Veit Bayer[1]

[1] DYNARDO – Dynamic Software and Engineering GmbH, Weimar, Germany

[2] ANSYS Germany GmbH, Otterfing, Germany

Abstract

Within the design development phases the Design for Six Sigma concept optimizes a design such that the products conform to Six Sigma quality. Which means that robustness and reliability are explicit optimization goals even with variations e.g. in manufacturing, design configuration and environment. The application of the reliability- and variance-based robust design optimization results in optimized designs such that they are insensitive to uncertainties up to a six sigma safety level. In this paper an efficient iterative decoupled loop approach is provided for reducing the necessary number of design evaluations. This is exemplary applied to a CAD and CAE parameter-based robust design optimization of an axial turbine, including manufacturing tolerances based on random field modeling.

The probabilistic and optimization tasks are performed with the optiSLang, SoS and SFrang software packages. Whereby, the CAE integration is realized by the ANSYS Workbench environment and optiPLug. In addition, the ANSYS Mechanical and CFD software offers a comprehensive solution for structural, thermal and fluid analysis. The software package also includes solutions for both direct and sequentially coupled physics problems including direct coupled-field elements and the ANSYS multi-field solver for supported physics, which is very efficient for tolerance interpolation of measurement data to different finite element meshes.

Keywords: robust design optimization, design for six sigma, robustness evaluation, reliability analysis, random fields, computational structural mechanics, fluid-strucutre interaction

*Contact: Dr.-Ing. Dirk Roos, DYNARDO – Dynamic Software and Engineering GmbH, Luthergasse 1d, D-99423 Weimar, Germany, E-Mail: dirk.roos[@]dynardo.de

1 Introduction

A large number of problems in manufacturing processes, production planning, finance and engineering design require an understanding of potential sources of variations and quantification of the effect of variations on product behaviour and performance. Traditionally, in engineering problems uncertainties have been formulated only through coarse safety factors. Such methods often lead to overdesigned products. Otherwise, the application of the deterministic optimization often results in designs with high imperfection sensitivities (oversensitivity designs) and non-robust and unsafe (underdesigned products) behaviour because the deterministic optimal design is frequently pushed to the design space boundary. The design properties have no room for tolerances or uncertainties.

Because of that, an integration of the assessment of robustness, reliability and safety into the optimization is necessary. Within the robust design optimization the design parameters can be random variables themselves and in addition the objective and the constraint functions can be random types. Using the robust design optimization we obtain robust optimized designs such that they are insensitive to uncertainties within a safety level of two sigma. The reliability-based optimization includes the failure probability as constraint condition or as term of the objective function themselves. So we obtain designs with minimal failure probability applicable for all safety levels up to 6 sigma.

There exist physical or geometrical quantities which vary randomly along the geometry of a structure, such as distributed loads, Young's modulus, material thickness etc. The spatial correlation of such parameters can be taken into account by modeling them as random field.

Computational fluid dynamics (CFD) is an engineering method in which flow fields and other physics are calculated in detail for an application of interest. ANSYS uses a multidisciplinary approach to simulation in which fluid flow models integrate seamlessly with other types of physics simulation technologies. The CFD, or fluids simulation, results can be used as part of a Simulation Driven Product Development (SDPD) process to illustrate how a product or process operates, to troubleshoot problems, to optimize performance and to design new products.

2 Successive robust design optimization

2.1 Robust design optimization

Design for Six Sigma is a concept to optimize the design such that the parts conform with six sigma quality, i.e. quality and reliability are explicit optimization goals. Robust design is often synonymous to "Design for Six Sigma" or "reliability-based optimization". The possible sigma levels start at 1 to 2 σ (variance-based robust design optimization) and go up to 6 σ (reliability-based robust design optimization) (Koch et al. (2004)), as shown in Table 1.

Structural designs within the sigma level $\leq \pm 2\sigma$ are characterized as "robust design". Therefore, the objective of the robust design optimization (e.g. Hwang et al. (2001); Ben-Tal and Nemirovski (2002); Doltsinis and Kang (2004)) is to find a design with a minimal variance of the scattering model responses around the mean values of the design parameters (see Byrne and Taguchi (1987); Phadke (1989)).

Sigma level	Percent variation	Probability of failure $P(\mathcal{F})$
1 σ	84.134474607	$1.59 \cdot 10^{-01}$
1.5 σ	93.319279873	$6.68 \cdot 10^{-02}$
2 σ	97.724986805	$2.28 \cdot 10^{-02}$
2.5 σ	99.379033467	$6.21 \cdot 10^{-03}$
3 σ	99.865010197	$1.35 \cdot 10^{-03}$
3.5 σ	99.976737092	$2.33 \cdot 10^{-04}$
4 σ	99.996832876	$3.17 \cdot 10^{-05}$
4.5 σ	99.999660233	$3.40 \cdot 10^{-06}$
5 σ	99.999971335	$2.87 \cdot 10^{-07}$
5.5 σ	99.999998101	$1.90 \cdot 10^{-08}$
6 σ	99.999999901	$9.87 \cdot 10^{-10}$

Figure 1: Sigma levels depending on the variation of the normal distribution correspond with defects per million and associated probability of failure $P(\mathcal{F})$ (assumption: normal distribution for all important random responses).

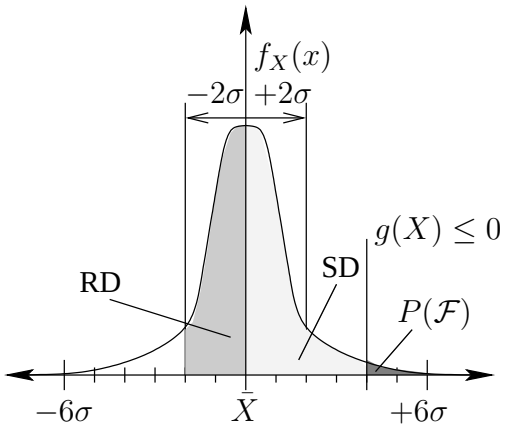

Figure 2: Normal distribution $f_X(x)$ with lower and upper specification limit on 2σ and 6σ level. Robust design (RD) and safety design (SD) ($\geq \pm 2\sigma$) depending on chosen limit state function $g(X) \leq 0$, e.g. stress limit state.

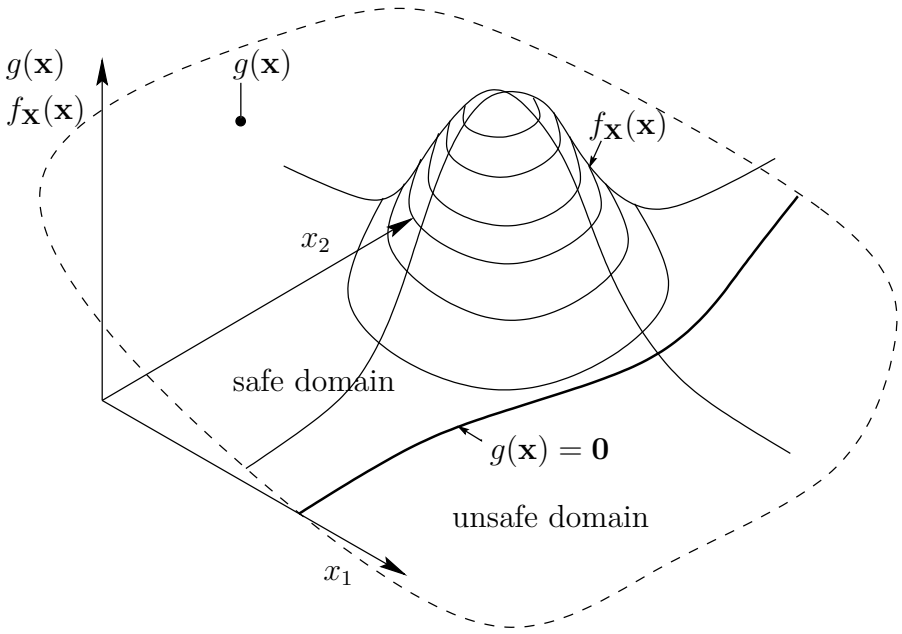

Figure 3: The state function $g(\mathbf{x})$ of a numerical model is given implicitly, e.g. is result of a finite element analysis depending on several design responses. The failure condition leads to a unknown deterministic limit state function $g(\mathbf{x}) = 0$, where $f_{\mathbf{X}}(\mathbf{x})$ is the joint probability density function.

In the reliability-based robust design optimization, the optimization problem can be enhanced by additional stochastic restrictions ensuring that prescribed probabilities of failure can not be exceeded, for example $P(\mathcal{F}) \leq 3.4 \cdot 10^{-6}$. Using the normal distribution assumption a probability of 3.4 out of 1 million is achieved when the performance target is 4.5 σ away from the mean value (short term). Of course, this assumption can be only used as a rough estimation of the safety level and we have to calculate the probabilities of failure using the reliability analysis, as shown e.g. in Roos et al. (2006). However, the optimized design which meets these conditions is often called as "Six Sigma Design" or "safety design". Usually, the robust design optimization problem

$$\begin{aligned} f(d_1, d_2, \ldots d_{n_d}, \sigma^2_{X_1}, \sigma^2_{X_2}, \ldots \sigma^2_{X_{n_r}}, P(\mathcal{F})) &\rightarrow \min \\ g_k(d_1, d_2, \ldots d_{n_d}) &= 0;\ k = 1, m_e \\ h_l(d_1, d_2, \ldots d_{n_d}) &\geq 0;\ l = 1, m_u \\ d_i &\in [d_l, d_u] \subset \mathbb{R}^{n_d} \\ d_l &\leq d_i \leq d_u \\ d_i &= E[X_i] \end{aligned} \tag{1}$$

with n_r random parameters $\mathbf{X}$ and n_d means of the design parameters $\mathbf{d} = E[\mathbf{X}]$ is enhanced by additional m_g random restrictions

$$\int_{g_j(\mathbf{x}) \leq 0} \overset{n_r}{\ldots} \int f_{\mathbf{X}}(\mathbf{x}) d\mathbf{x} - P(\mathbf{X} : g_j(\mathbf{X}) \leq 0) \leq 0;\ j = 1, m_g \tag{2}$$

with the joint probability density function of the basic random variables $f_{\mathbf{X}}(\mathbf{x})$ and m_g limit state functions $g_j(\mathbf{x}) \leq 0$ (see Figure 3) and the probability of failure $P(\mathcal{F})$

$$P(\mathcal{F}) = \int_{g_j(\mathbf{x}) \leq 0} \overset{n_r}{\ldots} \int f_{\mathbf{X}}(\mathbf{x}) d\mathbf{x} \tag{3}$$

and the variances

$$\sigma^2_{X_i} = \frac{1}{M-1} \sum_{k=1}^{M} \left(x_i^k - \mu_{X_i} \right)^2$$

is solved as a combination of a deterministic optimization in the design space and a stochastic analysis in the space of the random influences for every deterministic design.

This procedure leads in general to an inefficient double loop with a large number of design evaluations, e.g. finite element analysis. Furthermore, in real case applications of the virtual prototyping process, it is not always possible to reduce the complexity of the physical models and to obtain numerical models which can be solved quickly. Usually, every single numerical simulation takes hours or even days. Although the progresses in numerical methods and high performance computing, in such cases, it is not possible to explore various model configurations. An overview about advanced methods to solve robust design optimization problems can be found e.g. in Roos (2008). However, their use is restricted to problems with few random and optimization variables.

2.2 Successive robust design optimization

The most general way for reducing the required number of design evaluations is the application of an iterative decoupled loop approach (see e.g. Chen et al. 2003) in combination

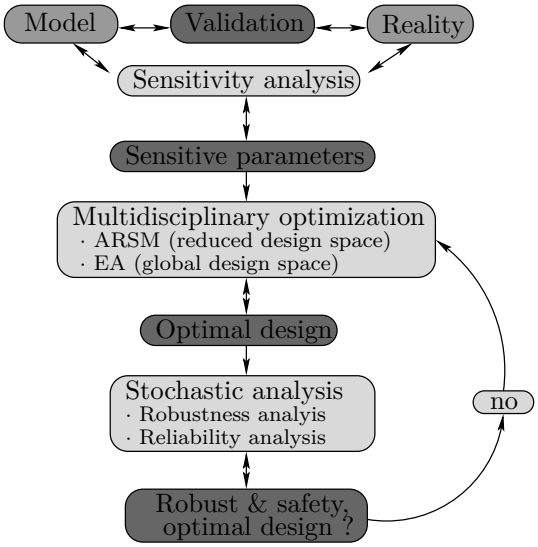

Figure 4: Basic concept of a successive robust design optimization.

with identification of the most significant random and design variables using the multivariate statistic within the sensitivity analysis or robustness evaluation. According the flow diagram in Figure 4, in a first step the sensitivity analysis can be used to prove the predictive capability of the simulation model and to identify the most important design parameters to solve the deterministic optimization problem, efficiently. After that, it is necessary to evaluate robustness and safety of the design at the current deterministic optimum.

Afterwards the deterministic formulation of the constraints and the objectives is to modify according to the achieved robustness, reliability or sigma level and the deterministic optimization is to be repeated until the requirements in terms of robustness and safety are fulfilled. Although, the optimization and reliability analysis runs mostly efficient in the space of the current significant parameters. So every size of problem definition (number of design and random parameters) is solvable for all kind of robustness values in combination with the consideration of the failure probability within all sigma levels. Furthermore, this proceeding allows highly flexible user interactions at every iteration step. At any time, the user can adapt the optimization problem with respect to the optimization goals, constraints and model configurations and can add additional requirements as a result of the advanced virtual design processes. However, for a global variance-based robustness analysis (see e.g. Bucher 2007) it is recommended to scan the design space using stochastic sampling methods and to estimate the sensitivity using the multivariate statistic based on surrogate models (for detailed reading see DYN 2009).

Results of a global variance-based sensitivity study are the most significant parameters of the optimization or random variables due to important model responses. So, it is possible to identify the sub domains and very efficient adaptive approximation methods can be used for optimization and reliability analysis (Roos and Ochsenfahrt 2009).

3 Random fields

3.1 Stochastic models

There exist three different views on random fluctuations of system properties:

- Single random variables X provide a stochastic model for the natural fluctuation of single parameters, such as CAD model parameters, material constants, or process parameters. They are characterized by a distribution type and statistical moments (e.g., the mean value μ_X and variance σ_X^2). Random variables may be pairwise correlated. Pearson's correlation coefficient is a statistical measure for a supposed linear relationship between two random variables. A random vector $\mathbf{X}$ is a compact mathematical notation for a set of several, possibly correlated, variables. The statistical moments are then pooled in the mean vector $\boldsymbol{\mu}_X$ and covariance matrix $\mathbf{C}_{XX}$.

- A random fluctuation over time is described as random process $X(t)$. A typical application is a transient loading. Here, the value of the quantity is a random variable at each observed point in time. The values at different time points may be, again, mutually correlated. For the special case of white noise all time points are independent from all others.

- In order to characterize and model random fluctuations over space, the methodology of random fields is applied. Any manufacturing process (e.g., metal forming, casting) causes deviations from the design geometry or a scatter of material properties within the structure. These cannot be modelled in a meaningful way by single variables like CAD parameters. Hence modelling and simulation of random fields will be described briefly in the following.

The stochastic analysis software SLang (– the Structural Language) includes several methods solving all stochastic models, including random fields and random processes. Currently, optiSLang (– the optimizing Structural Language) supports methods to solve nonlinear optimization and to analyse random variables only. In addition, the SoS (– Statistics on Structures) add-on tool to optiSLang provides methods to solve random fields.

3.2 Random fields

Regard a local vector $\mathbf{r} \in \mathbb{R}_{Str.}$ pointing to a location in space, the domain $\mathbb{R}_{Str.}$ is limited by the structure observed in an application. A random field is a random function $X(\mathbf{r})$, i.e. the value of X at any point $\mathbf{r}$ is itself a random variable, as shown in Figure 5. As any random variable, it is characterized by a probability distribution function, which can be parameterized by distribution type and stochastic moments. For random fields, the moments become functions over space as well. In particular

$$\mu_X(\mathbf{r}) = \mathrm{E}[X(\mathbf{r})] = \int_{-\infty}^{+\infty} x f_X(\mathbf{r}, x)\, dx \tag{4}$$

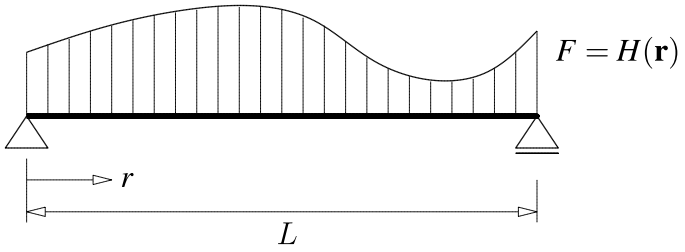

Figure 5: Random fluctuation of any property $H(\mathbf{r}) = X(\mathbf{r})$ over space, e.g. load (wind field), manufacturing tolerances (geometry, material), etc.

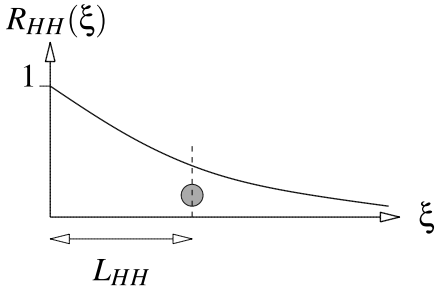

Figure 6: Correlation function and correlation length of the random fluctuation $H(\mathbf{r})$.

denotes the *mean function*, and

$$\begin{aligned} C_{XX}(\mathbf{r}_1, \mathbf{r}_2) &= \mathrm{E}\left[\Big(X(\mathbf{r}_1) - \mu_X(\mathbf{r}_1)\Big) \cdot \Big(X(\mathbf{r}_2) - \mu_X(\mathbf{r}_2)\Big)\right] \\ &= \int_{-\infty}^{+\infty}\int_{-\infty}^{+\infty} x_1 x_2 f_X(\mathbf{r}_1, \mathbf{r}_2, x_1, x_2)\; dx_1\; dx_2 - \mu_X(\mathbf{r}_1)\mu_X(\mathbf{r}_2) \end{aligned} \tag{5}$$

the *auto-covariance function*, with E[.] being the expected value operation. If the auto-covariance function is normalized as $\rho(\mathbf{r}_1, \mathbf{r}_2) = C_{XX}(\mathbf{r}_1, \mathbf{r}_2)/C_{XX}(\mathbf{r}_1 = \mathbf{r}_2)$, one obtains the spatial function of Pearson's correlation coefficients, which indicates the amount of linear dependency between the random properties at two locations. The so-called *correlation length* L_{XX}, which is actually the centre of gravity of the correlation function, is a typical characteristic of the correlation coefficient function, as shown in Figure 6. It has to be estimated from manufacturing processes, natural scatter of material properties, etc.

3.3 Modelling

For computational analyses, a random field has to be discretized. Typically, the nodes of the underlying Finite Element model are used as supports for displacement or coordinate fields, element mid points or integration points for material properties, stresses or strains. If measurements provide the data base for a random field model, a separate mesh of support points defines the discretization. After simulation, realizations of the random field then have to be mapped to the structural model by suitable interpolation for further analysis of the such generated imperfect structures.

Discretization leads to a finite set of random variables $\mathbf{X}$, characterized by a mean vector and a covariance matrix $\mathbf{C}_{XX}$. From now on, *Gaussian random fields with zero mean vector are considered only.* Then the covariance matrix suffices for the complete characterization of the random variables set. For the generation of realizations of the random field by Monte Carlo methods, independent random variables are required. They can be obtained by the expansion shown in the following. The procedure offers also the opportunity to assess given spatial data, identify the most relevant variables (with respect to criteria explained later) and reduce the problem dimension.

The random field is expanded by a series of deterministic shape functions scaled by random amplitudes. If the shape functions are orthogonal, it can be shown that the random amplitudes are independent. For this purpose, the covariance matrix is decomposed

by eigenvalue analysis:

$$\mathbf{\Psi}^T \mathbf{C}_{XX} \mathbf{\Psi} = \mathrm{diag}\{\lambda_i\} \tag{6}$$

Therein, $\mathbf{\Psi}$ is the matrix of eigenvectors of $\mathbf{C}_{XX}$ stored columnwise. The eigenvectors form the set of orthogonal shape functions. The random amplitudes are defined as

$$Y_i : \mathcal{N}\left(0, \sqrt{\lambda_i}\right) \tag{7}$$

The Karhunen-Loève expansion of the random field, shown in Papoulis (1991); Ghanem and Spanos (1991), in matrix notation reads

$$\mathbf{X} = \mathbf{\Psi} \ \ \mathbf{Y} \tag{8}$$

and relates the generalized variables $\mathbf{Y}$ generated by random sampling to the physically meaningful space spanned by $\mathbf{X}(\mathbf{r})$. Typical shape functions are shown in the context of the application example, Figures 51 ff.

The eigenvalues of the covariance matrix are usually stored sorted by magnitude in descending order. Because of eq. (7), this fact delivers a criterion for truncating the Karhunen-Loève series. Each eigenvalue considered contributes a part to the total variance of the random field which is the sum of diagonal elements of the covariance matrix. The quality of approximation of the random field is expressed by the variability fraction (Brenner 1995)

$$Q = \frac{\sum_{i=1}^{n} \sigma_{Y_i}^2}{\mathrm{trace}\left(\mathbf{C}_{XX}\right)} \ ; \quad 0 \leq Q \leq 1 \tag{9}$$

The number n of the random variables considered has to be adjusted before the simulation in order to reach a sufficient quality, e.g. $Q > 0.9$. A vast reduction of the problem dimension is possible that way. This opens the random field modelling to subsequent robustness and reliability analyses by advanced methods such as Importance Sampling or Adaptive Response Surface Method, which are typically sensitive towards dimension.

3.4 Relevance assessment of random field variables

Even if a truncated series expansion of a random field represents a large amount of the total variance, as computed by eq. (9), the random field representation may be not optimal for a reliability analysis, because it lacks those variables which contribute most to the performance of the application, or the random field model may still incorporate a too large set of variables. The dimension can be further reduced by selecting those random variables which contribute most significantly to the structural performance. Although a direct physical relation between random amplitudes, or their respective shape functions, and the performance criterion is difficult to find, a phenomelogical assessment is easily possible by methods of robustness assessment.

The Coefficient of Importance (CoI), see DYN (2009), allows a ranking of input variables by their contribution to the variance of the performance. The influence typically decreases strongly, therefore this gives a criterion for selection of input variables, which, in contrast to the above (eq. 9), takes into account the statistical relation between input and output. This selection has been shown to be superior to the simple input-related

criterion in reliability analyses of stability problems in Bayer et al. (2007); Bayer and Roos (2009).

In the application presented here, the performance function is approximated by the Metamodel of Optimal Prognosis – MOP – ((DYN 2009)) for the purpose of reliability analysis (sect. 5.8.3 ff.). The Coefficient of Prognosis (CoP) applied therefore is evaluated by computing mean square differences of a subset of supports of the metamodel and the directly computed performance. Hence the metamodel is based upon the input variables with the highest CoPs, among those operation parameters, material parameters and random amplitudes of the imperfect turbine blade surface. Also this selection criterion considers input-output relations.

4 Computational fluid dynamics and fluid structure interaction

4.1 Fluid structure interaction

For the simulation of many industrial applications multiple physical effects have to be taken into account. An important application is the interaction between the dynamics of a fluid flow and the structure of a solid body, commonly referred to as Fluid Structure Interaction (FSI). One kind of interaction is the influence of the fluid pressure force or the fluid heat flow on the attached structure. In addition, the structural deformation can have a reverse impact on the flow, e.g. by imposing the fluctuating motion based on the structural eigenmodes for the flow computation. Another example for a strong interaction between flow and structure is aero-elasticity which typically requires an implicit solver coupling. Depending on the application different solution strategies and solver coupling methods may be required. ANSYS Workbench provides an integrated simulation environment which is capable to compute a variety of field coupling scenarios. For FSI applications the ANSYS finite element solver is used for the structural analysis and coupled with the ANSYS CFX flow solver, which is used for the fluid analysis. The individual solver capabilities to predict the different effects are combined in a multi-field simulation environment, and the way of coupling between the solvers can be adjusted to the simulation problem. Communication and data transfer is handled consistently inside ANSYS Workbench.

4.2 Process integration

Typically, there are two ways for integration of arbitrary external CAD and CAE programs. First, reading and writing of parametric data to and from ASCII input and output files, is the most general way to doing integration of any engineering processes. The second way provides CAD-based parametrization using bidirectional interfaces to binary input and output parameters.

Therefore exit several optiSLang interfaces, e.g. for ANSYS, ABAQUS, CATIA and EXCEL. Within the application example we used the optiPLug interface to ANSYS Workbench, as shown in Figure 7. ANSYS Workbench reads and writes binary data to and from many CAD software in order to explore a wide range of responses. Within Workbench all input and output parameters are created. The optiPLug interface creates an

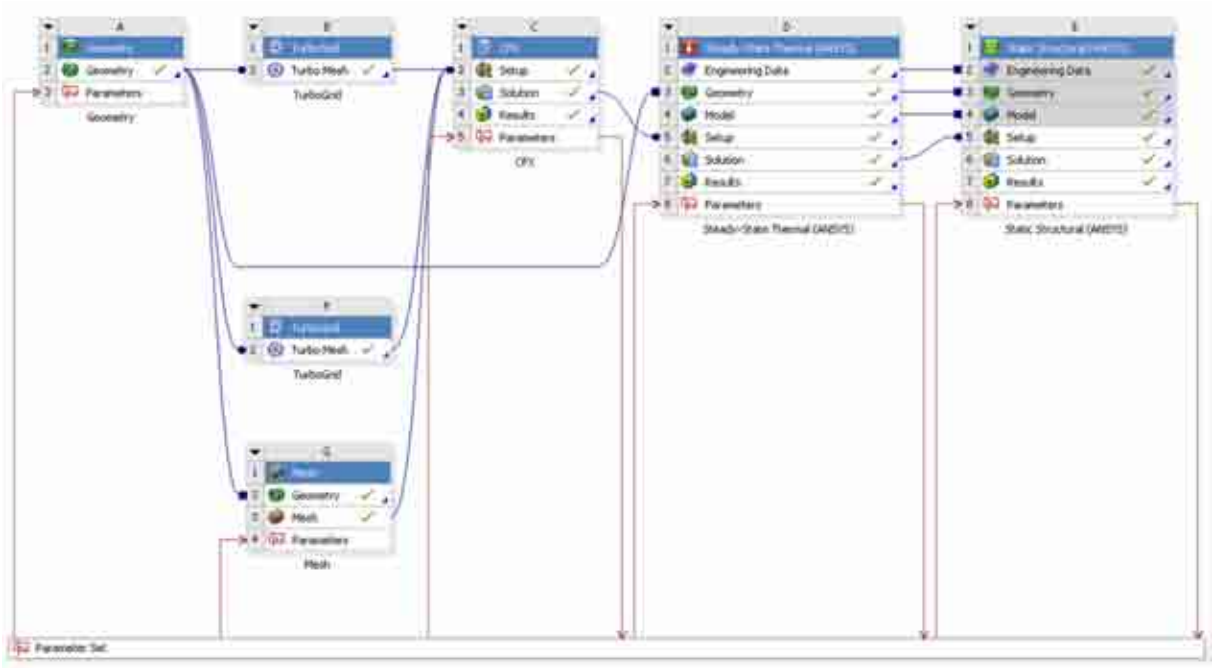

Figure 7: Definition of parameters and optimization task and process integration of arbitrary CAD and CAE tools in the context of optimization and stochastic analysis. Binary-based CAE parameter definition within the ANSYS Workbench environment and using the optiPLug interface of optiSLang.

optiSLang project with predefined parameter descriptions and writes and reads the current parameters and responses. Furthermore, optiSLang starts Workbench as a batch process, if necessary using parallel distribution of several Workbench processes.

5 Application example

5.1 Design for six sigma of the turbine engine

The Figure 8 shows a typical turbine engine used in power plants or aircraft engines. Since the engineering of turbo machinery the improvement of specific physical behavior, especially the efficiency, is one of the key issues. In conventional engineering the design is improved by evaluating design response and making design changes based on experience, intuition or guess. Due to the introduction of virtual prototyping the turbo machinery analysis have a very high degree of complexity and desired improvements are hard to reach with conventional trial and error procedure. A modern approach to search for better designs or to compute the 'best' design has to introduce all available engineering know how and has to automate a multidisciplinary optimization process. An other important issue is the robustness of a turbo machinery, while operating an constant value of several parameter is needed, since the geometry is not manufactured perfect and some other parameter will vary in the real approach.

To prove the reliability of the initial design we used the robustness analysis to estimate the sigma level. And the robust design optimization is used to increase the efficiency, power and reliability to get an optimized six sigma design.

Figure 8: Axial gas turbine.

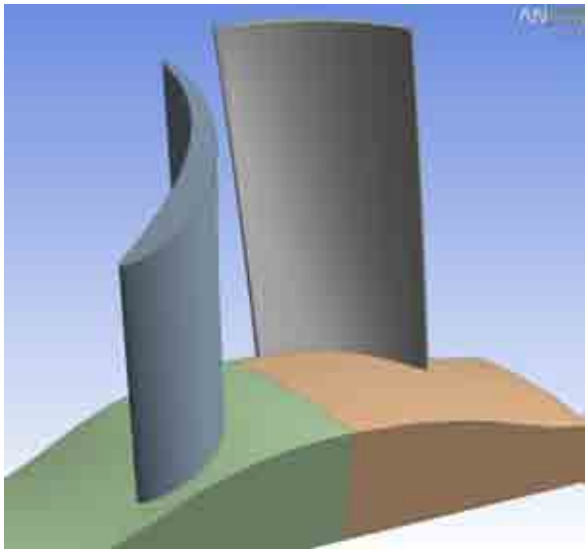

Figure 9: ANSYS DesignModeler geometry model of the passage of one stage of an axial gas turbine, used for CHT and FEA.

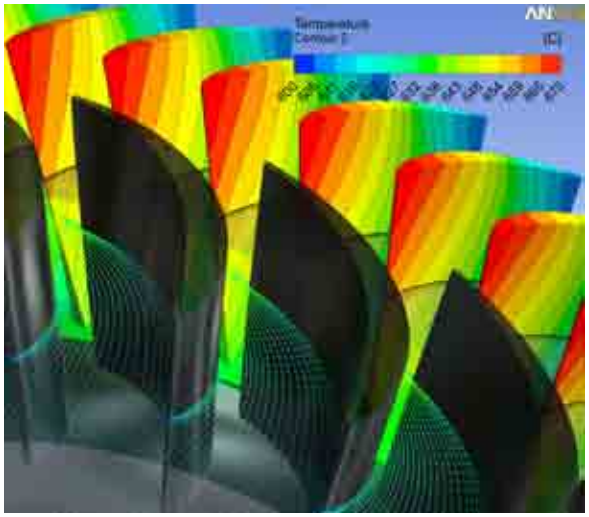

Figure 10: Result of the CHT calculation with temperature distribution of the rotor blade (vector plot of the gas velocity in mid-span).

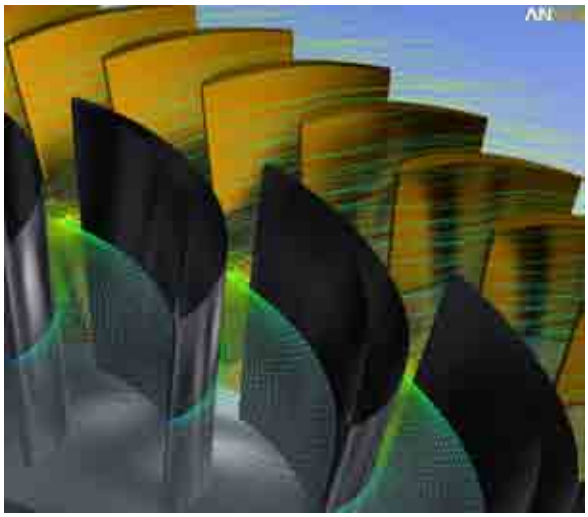

Figure 11: Result of the CHT calculation (vector plot of the gas velocity in mid-span and stream lines).

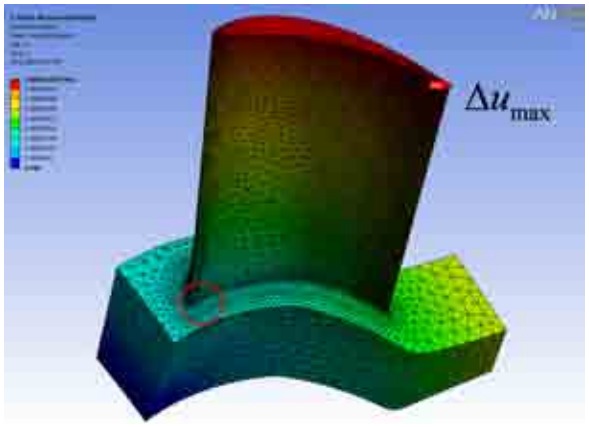

Figure 12: Displacements of the FEA of the rotor blade.

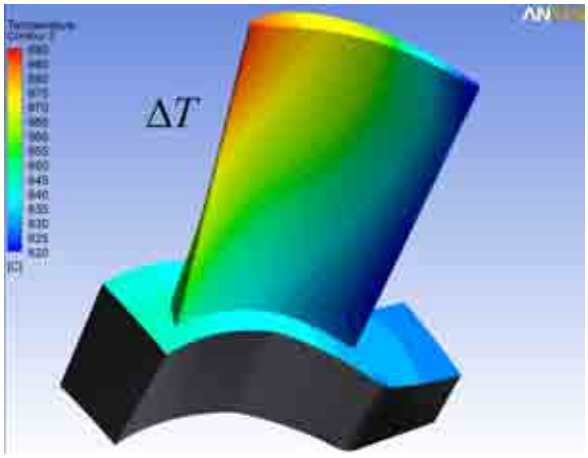

Figure 13: Mapped temperature field, as a result of CHT (see Pictures 10), to the FEA mesh of the rotor blade.

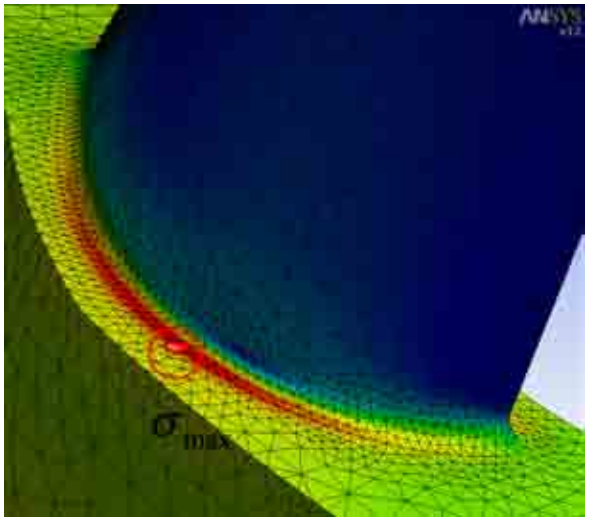

Figure 14: Equivalent von Mises stress distribution of the FEA of the rotor blade. The maximal stress is located near the design parameter Rotor blend radius.

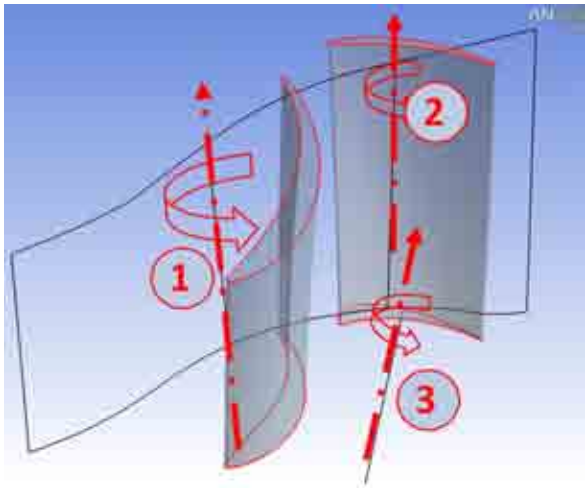

Figure 15: Design parameters: Blade angle (Guide vane), Blade angle (Shroud profile) and Blade angle (Hub profile).

Table 1: Performance relevant output parameters of the model responses, target function definition and constrains or limit states, respectively.

Response parameters, weighted target function $p(\mathbf{x})$, constraint functions (limit state conditions) $g(\mathbf{x})$ for robustness and reliability analysis.				
	Description/Symbol	Name	Initial value	Unit
1	Total temperature ratio $\Theta_T = T_{t,\text{Inlet}}/T_{t,\text{outlet}}$	`Ttratio`	1.1158	
2	Torque M_p	`myTorque`	-576.75	Nm
3	Isentropic efficiency $\eta = f(\Theta_T, \Pi_p)$	`myeta`	0.71645	
4	Total pressure ratio $\Pi_p = p_{t,\text{Inlet}}/p_{t,\text{outlet}}$	`ptratio`	1.6738	
5	Power at rotor P	`myPower`	$1.2079 \cdot 10^6$	W
6	Maximal temperature	`Temperature_Maximum`	688.017	°C
7	Maximal total deformation	`Total_Deformation_Maximum`	$6.3588 \cdot 10^{-4}$	m
8	Maximal v. Mises stress $\sigma_{\max}$	`Equivalent_Stress_Maximum`	$2.1865 \cdot 10^9$	Pa
9	Thermal conductivity	`Thermal_Conductivity`	60.5	W/m/°C
10	Mass flow rate $\dot{m} = f(\Pi_p, \alpha_{\text{GV}})$	`myMassFlow`	11.5655	kg/s
	Objective function $p(\mathbf{x})$ (see Equ. 10)	`myetaObj`	1.25	
	Constrains for stresses			
1	$g_1(\mathbf{x}) = \sigma_{\max} \leq 2.8 \cdot 10^9$ for efficiency			Pa
2	$g_2(\mathbf{x}) = \eta \geq 0.795$ and power			
3	$g_3(\mathbf{x}) = P \geq 1 \cdot 10^6$			W

Table 2: Design parameters.

Upper and lower bounds x^u, x^l of the optimization parameters.						
	Description	Name	Symbol	x^l	x^u	Unit
1	Rotational velocity of the rotor	`myomega`	Ω	-2400	-1600	rad/s
2	Blade angle (Hub profile)	`DS_hub_angle`	α_{Hub}	-1.0	1.0	°
3	Blade angle (Shroud profile)	`DS_shroud_angle`	α_{Shroud}	-3.5	3.5	°
continued on next page ...						

	Description	Name	Symbol	$E(X)$	σ_X	Unit
4	Blade angle (Guide vane)	`DS_gv_angle`	α_{GV}	-12.0	3.0	°
5	Total temperature inlet	`Ttin`	$T_{t,\mathrm{Inlet}}$	995	1005	K
6	Total pressure inlet	`ptin`	$p_{t,\mathrm{Inlet}}$	295000	305000	Pa
7	Rotor blend radius	`DS_FBlendRotor`	r	0.9	1.1	mm

5.2 Model description, design parameters, objective function and limit states

The Figure 9 shows the CAD model of the turbine blades. The geometry of the rotor is defined by the hub and shroud profile of the initial design. Both, hub and shroud, can be rotated around an axis, Fig 15. The blade shape is finally given by staggering the given/modified profiles. The guide vane can also be rotated about an axis, while the shape remains constant. In this sense three parameters are important for the blade design. The maximal stress is assumed at the blend of the rotor blade, thus the radius is an additional parameter. The boundary conditions for the fluid flow are the rotational velocity of the rotor, total pressure p_t and total temperature T_t at the inlet and static pressure p_s at the outlet. Additionally the influence of all material properties is to identified.

The performance-relevant response parameters are compiled in the Table 1. The target of the optimization process is to maximize the efficiency η and power P of the turbine engine with respect to a limitation of the maximal v. Mises stress $\sigma_{\max}$. Often, multidisciplinary optimization problems are governed by multiple objectives. Then part of the solution strategy of a multidisciplinary optimization problem is the definition or selection of the best compromise objective function from a set of multiple and frequently conflicting objectives.

Depending on the optimization strategy, sometimes only the dominant objective should be defined as an objective, and the other objectives should be defined as constraints. But more often, the compromise (or preference) objective function will be defined as a combination

$$p(f_i(x_1, x_2, \ldots x_{n_d})) \rightarrow \min$$

of $i = 1, ..., m$ multiple weighted objectives and constrains. In this case, the definition of the priority (or weight) attached to each objective is not a trivial task. Moreover, there may be no clearly defined decision base which objectives are more or less important. So, the optimization is sometimes an iterative search of the best weights for the objectives. In addition to the weights, it is recommended to scale the objective function terms

$$p(f_i(x_1, x_2, \ldots x_{n_d})) = \sum_{i=1}^{m} W_i \left(\frac{f_i(\mathbf{x})}{\Gamma_i} \right)$$

and applied to this example

$$p(\mathbf{x}) = 1.0 \frac{1-\eta}{\Gamma_1} + \frac{1}{4} \frac{1}{\Gamma_2} \left(1 - \frac{P}{2 \cdot 10^6} \right) \tag{10}$$

with the weights $W_1 = 1$, $W_2 = 0.25$ and normalization factors $\Gamma_1 = 0.28355$, $\Gamma_2 = 0.396$ for normalization according to the start design. The $n_d = 7$ design geometry and process parameters $\mathbf{x}$ of the optimization problem are compiled in the Table 2 with the upper and lower bounds x_i^u, x_i^l. Whereby the feasible design area is restricted by the defined constrains, as shown in Table 1.

5.3 Structural, thermal and fluid analysis

ANSYS Workbench is an adaptable and modular CAE environment which allows different tasks for many types of simulation including FSI. It serves as the integration platform for all ANSYS tools, but can also be used for in-house codes and third party software. The main goal of ANSYS Workbench is to provide a complete platform for upfront simulation which then drives product development. It allows standard components analyses but also the simulation of complete systems which in many cases requires multi-physics capabilities. The underlying data structures and the unified user interface allow for new and unique CAE simulation capabilities on the same geometry model. In that respect ANSYS Workbench makes virtual prototyping become reality. Fig. 7 shows schematically existing tools of ANSYS Workbench, which have a relevance for an FSI simulation. This Workbench infra stucture is used to include the data of the Random Field, generated by SoS, into the ANSYS structural solver and ANSYS CFX. Finally, the environment can be customized depending on the individual needs of an application. ANSYS Workbench provides a consistent infrastructure which allows to use the same geometry model for different types of simulation and to exchange data between different solvers internally. This is the basis for an efficient and reliable FSI simulation. Depending on the type of application different coupling strategies may be required. In principle, any type of solver coupling can be grouped into a sequential or a simultaneous coupling. Sequential coupling is defined as a simulation where individual solver runs are carried out in sequential order. The main advantage of a sequentially coupled system is that the computational effort is of the same order as for the single physics application. The data is transferred either from the structural analysis to the flow solver or in the opposite direction as shown schematically in Fig. 7. The solution of one field is used as an initial condition or a boundary condition for the subsequent simulation. If during the simulation the data exchange is performed only once, i.e. there is only a one way impact from the structural analysis on CFD or vice-versa, then the process is termed a one-way coupling. In this case the influence of the structural deformations on the fluid flow can be negled, i.e. we have a one-way coupling.

5.4 Evaluate the robustness of the initial design

The robustness evaluation is used to estimate the robustness and safety level (see Table 1) of the initial design introducing uncertainties of geometry, material, process and environment, as shown in Table 3.

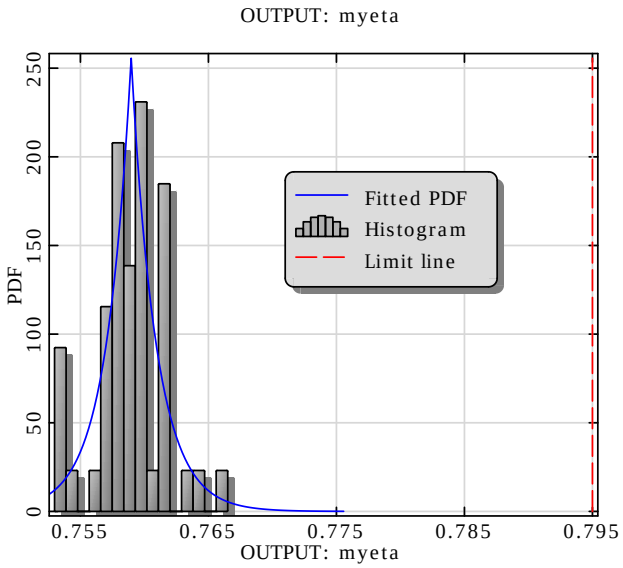

Statistic data			
Min:	0.753	Max:	0.7665
Mean:	0.759	Sigma:	0.002767
CV:	0.003645		
Skew ness:	-0.1759	Kurtosis:	3.679
Fitted PDF: Laplace			
Mean:	0.759	Sigma:	0.002767
Limit x = 0.795			
P_rel =	1	P_fit =	1
Probability P(X<x) = 0.95			
x_rel =	0.763049	x_fit =	0.763471

Figure 16: Histogram of η with mean and standard deviation and estimated $P(\mathcal{F}) = 1.00$.

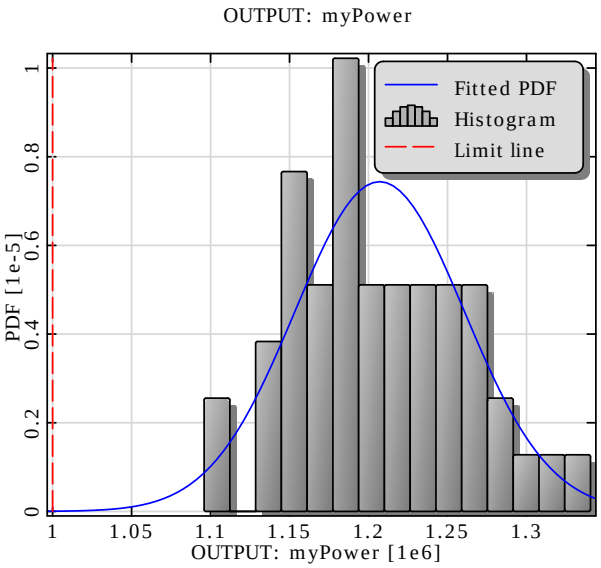

Statistic data			
Min:	1.096e+06	Max:	1.341e+06
Mean:	1.207e+06	Sigma:	5.364e+04
CV:	0.04444		
Skew ness:	0.2879	Kurtosis:	2.766
Fitted PDF: Normal			
Mean:	1.207e+06	Sigma:	5.364e+04
Limit x = 1e+06			
P_rel =	0	P_fit =	5.67009e-05
Probability P(X<x) = 0.95			
x_rel =	1.29529e+06	x_fit =	1.29528e+06

Figure 17: Histogram of P with mean and standard deviation and estimated $P(\mathcal{F}) = 5.67 \cdot 10^{-05}$.

Table 3: Uncertainties of geometry, material, process and environment

Random parameters with normal distribution type, mean value $E(X)$ and standard deviation σ_X						
	Description	Name	Symbol	$E(X)$	σ_X	Unit
1	Rotational velocity of the rotor	`myomega`	Ω	-2094.39	41.8878	rad/s
2	Blade angle (Hub profile)	`DS_hub_angle`	α_{Hub}	0.0	0.00674	°
3	Blade angle (Shroud profile)	`DS_shroud_angle`	α_{Shroud}	0.0	0.00357	°
4	Blade angle (Guide vane)	`DS_gv_angle`	α_{GV}	0.0	0.1947	°
5	Total temperature inlet	`Ttin`	$T_{t,\text{Inlet}}$	1000	207	K
6	Total pressure inlet	`ptin`	$p_{t,\text{Inlet}}$	300000	90007	Pa
7	Pressure outlet	`pout`	p_{out}	87000	17407	Pa
8	Specific heat capacity at constant pressure, air	`myAirCP`	$c_{p,a}$	1004.4	30.1327	J/kg/K
9	Specific gas constant	`myAirR`	R	287.102	8.6131	J/kg/K
10	Specific heat capacity, steel	`mySteelCP`	$c_{p,s}$	434	21.77	J/kg/K
11	Density of the steel material	`mySteelDensity`	ρ	7850	78.57	kg/m^{-3}
12	Heat conductivity, steel	`mySteelLambbda`	λ	60.5	2.427	W/m/K
13	Rotor blend radius	`DS_FBlendRotor`	r	1.0	0.027	mm
14	Youngs‘ modulus	`Youngs_Modulus`	E	$2 \cdot 10^{11}$	$6 \cdot 10^9$	Pa
15	Poissons ratio	`Poissons_Ratio`	ν	0.3	0.17	

The robustness evaluation is based on an optimized latin hypercube sampling procedure with $N = 48$ design evaluations with 2 failed designs. According the required number of simulations

$$N \geq \frac{10}{P(\mathcal{F})}$$

the direct calculation of the failure probability is limited to $P(\mathcal{F}) \geq 0.208$ (0.815 σ). But the statistic in terms of a “second moment representation” of the response parameters can be explained by the $N = 48$ samples regarding the histogram of the response parameters. Mean and standard deviation can be used to evaluate the sigma level

$$\sigma_L = \frac{g(\mathbf{X}) - E[\mathbf{X}]}{\sigma_{\mathbf{X}}} \tag{11}$$

according the defined limit state conditions $g(\mathbf{X})$ given in Table 1. Using the assumption of normal distribution for all important random responses we obtain a rough estimation

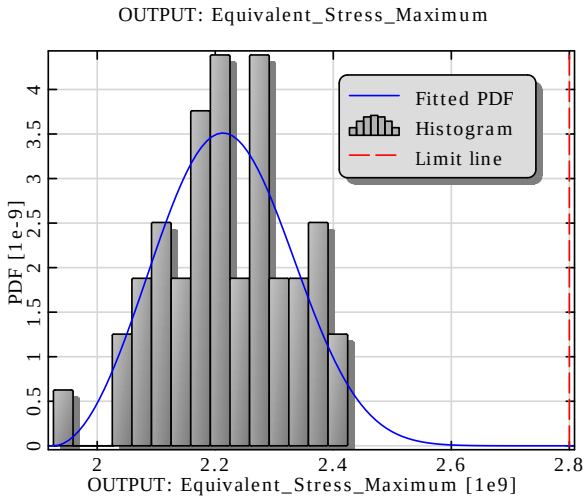

Statistic data			
Min:	1.926e+09	Max:	2.424e+09
Mean:	2.221e+09	Sigma:	1.086e+08
CV:	0.04892		
Skew ness:	-0.2418	Kurtosis:	2.725
Fitted PDF: Extreme Typ III (Max) Weibull			
Mean:	2.221e+09	Sigma:	1.086e+08
Low er cut:	1.926e+09		
Limit x = 2.8e+09			
P_rel =	1	P_fit =	1
Probability P(X<x) = 0.95			
x_rel =	2.38676e+09	x_fit =	2.40465e+09

Figure 18: Histogram of $\sigma_{\max}$ with mean and standard deviation and estimated $P(\mathcal{F}) = 0.00$.

Limit state condition	Sigma level σ_L	$P(\mathcal{F})$ (Equ. 12)	$P(\mathcal{F})$ (PDF)
$g_1(\mathbf{x}, \sigma_{\max})$	5.33σ	$4.91 \cdot 10^{-8}$	0.00
$g_2(\mathbf{x}, \eta)$	13.01σ	1.00^a	1.00
$g_3(\mathbf{x}, P)$	3.86σ	$5.67 \cdot 10^{-5}$	$5.67 \cdot 10^{-5}$

Figure 19: Sigma levels and associated probability of failure $P(\mathcal{F})$ of the initial design (assumption: normal distribution of the random response) and estimated $P(\mathcal{F})$ based on the fitted probability density function (PDF).

[a] Mean of η is located in the failure domain, so the assigned probability means the probability of surviving instead of the probability of failure which is $P(\mathcal{F}) = 1 - P(\mathcal{S})$

of the probability levels

$$P(\mathcal{F}) = P[\mathbf{X} : g(\mathbf{X}) \leq 0] \approx \Phi^{-1}(x : g(X) = 0) \tag{12}$$

as shown in Figure 19. Figures 16 to 18 show the histograms of power P, efficiency η and the maximal v. Mises stress $\sigma_{\max}$ including the limit state conditions. It is recommended to use the fitted distribution functions to estimate the failure probabilities within the sigma levels 1 to 3. The failure probabilities according the safety levels between 3 and 6 are predictable using the reliability analysis. The estimation of the failure probability using the distribution fits gives an unacceptable value of $5.67 \cdot 10^{-5}$ for violating the limit state condition regarding the power P and 100% for the efficiency η, particularly. Therefore, in the following robust design optimization the feasible design space has to be restricted to ensure an acceptable safety level.

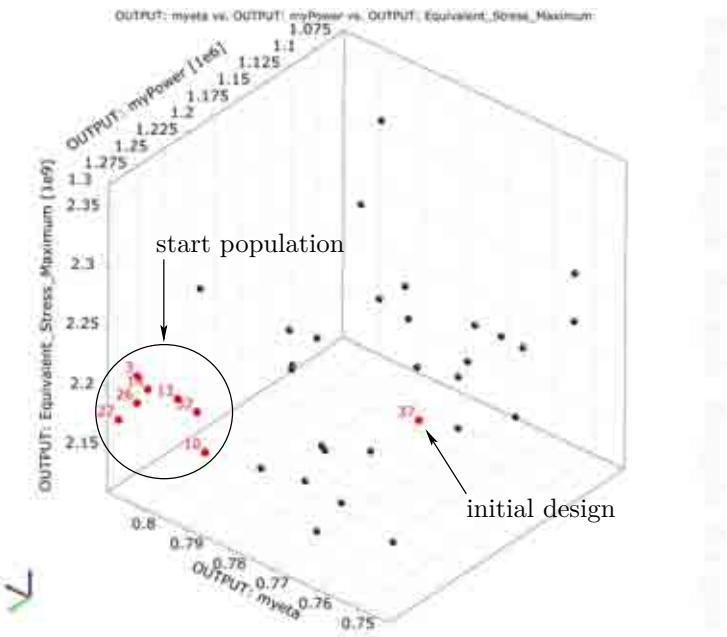

Figure 20: Anthill plot of the $N = 75$ latin hypercube results of the sensitivity analysis including the responses η, P and $\sigma_{\max}$ of the initial design. The best designs are selected as start population of the first evolutionary optimization step.

5.5 Sensitivity analysis of the initial design

The first most important step for a successful and efficient optimization procedure is to analyse the global sensitivities of the design parameters of the initial design. Introducing of lower and upper bounds of the design parameters, as shown in Table 2, an optimized latin hypercube sampling with N=75 design evaluations in parallel gives the anthill plots of all performance relevant response parameters η, P and $\sigma_{\max}$, as shown in Figure 20.

The matrix of the linear coefficients of correlation in Figure 21 shows only few input parameters for each response which have a strong linear correlation. The matrix shows only the statistical significant correlations greater than the statistical error of the simulated correlation of the input parameters. For practical applications it is recommended to prove the confidence intervals. These confidence levels I_p should perform the following conditions: $\rho \geq 0.5$: $I_p \leq 0.15$, e.g. $[-0.075; 0.075]$ and $\rho \geq 0.7$: $I_p \leq 0.10$, e.g. $[-0.05; 0.05]$. Otherwise, the number of design evaluations has to be increased. In our case, the confidence interval for correlation coefficients near $|\rho_{ij}| = 0.5$ is $[-0.06; 0.05]$ according to a 95% significance level. Which means that 95 of $N = 100$ sensitivity analyses would result in estimated correlation coefficients between 0.44 and 0.55. The confidence levels of the coefficients of correlation $|\rho_{ij}| = 0.5$ and 0.7 show the possibility to reduce the necessary number of design evaluation for the next sensitivity or robustness evaluations.

The adjusted value of coefficient of determination R^2_{adj} gives the amount of variance that can explained by a linear or nonlinear regression model including all significant input parameters and gives the optimization potential within the given design parameter boundaries. Figures 22 to 26 show the coefficient of determination for the objective terms η and P and the critical constraint $\sigma_{\max}$, depending on a linear regression model. An important prediction value to explain the influence of a single input parameter l on a

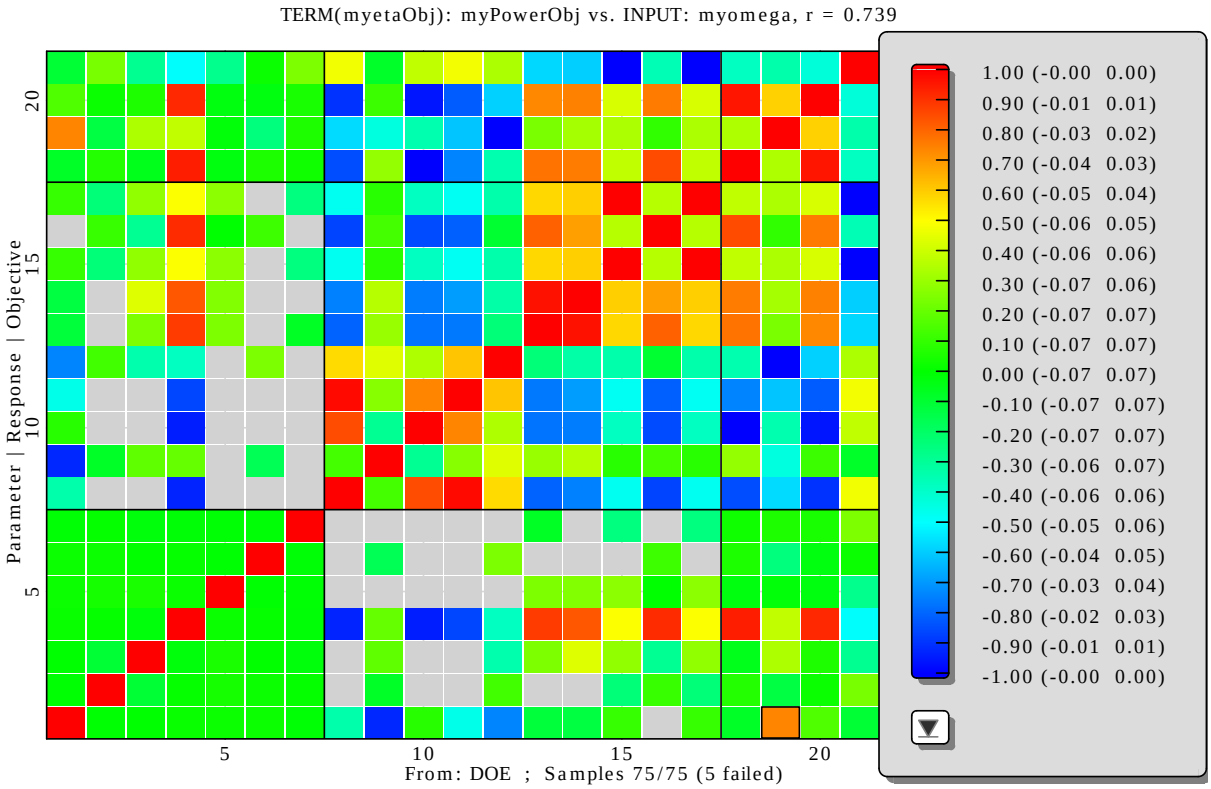

Figure 21: Matrix of the linear correlation (including the confidence levels) between design parameters, responses and objectives.

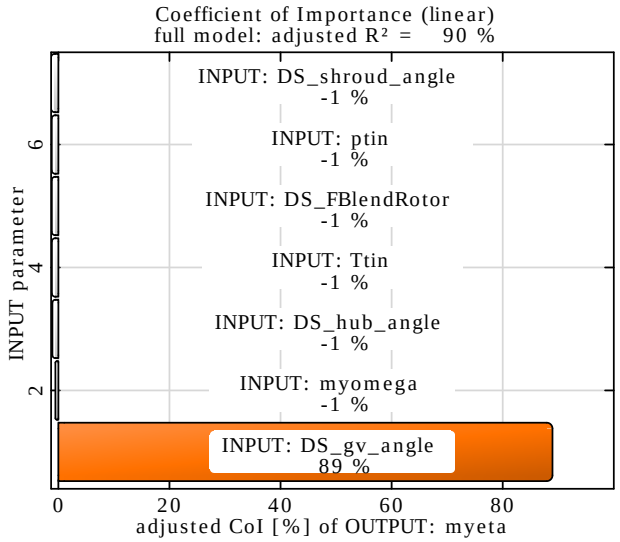

Figure 22: Adjusted value of coefficient of determination R^2_{adj} and coefficients of importance of the efficiency η.

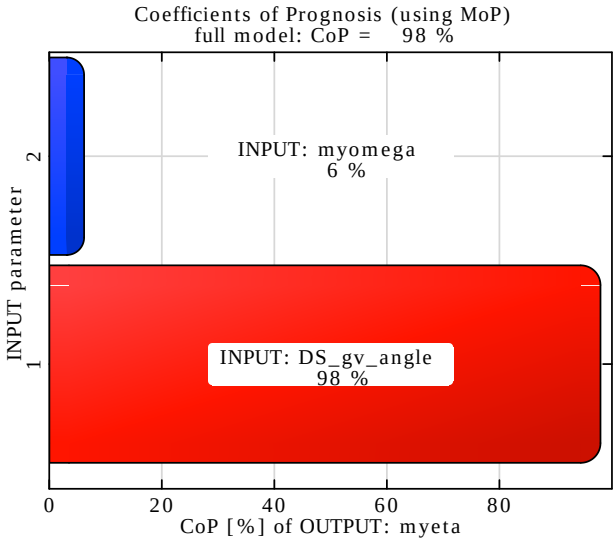

Figure 23: Coefficient of prognosis of the efficiency η.

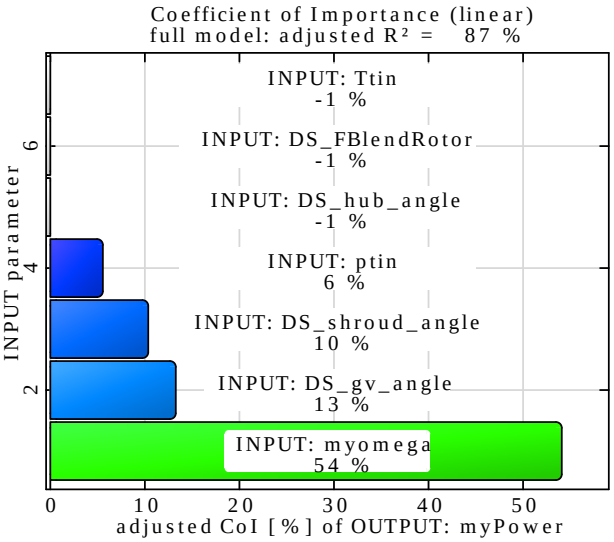

Figure 24: Adjusted value of coefficient of determination R^2_{adj} and coefficients of importance of the power P.

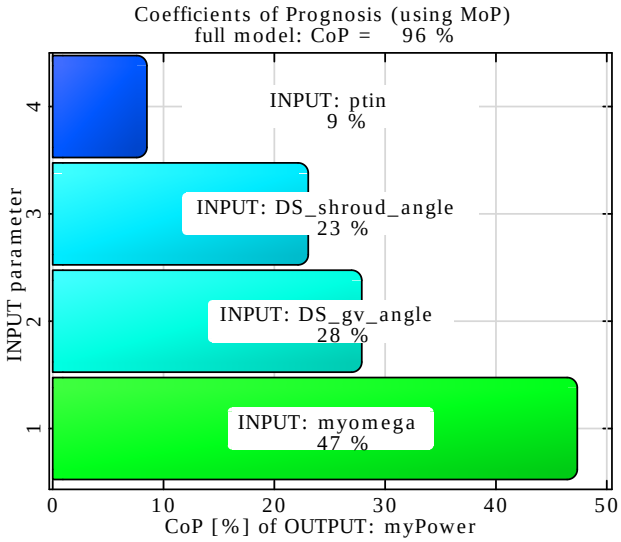

Figure 25: Coefficient of prognosis of the power P.

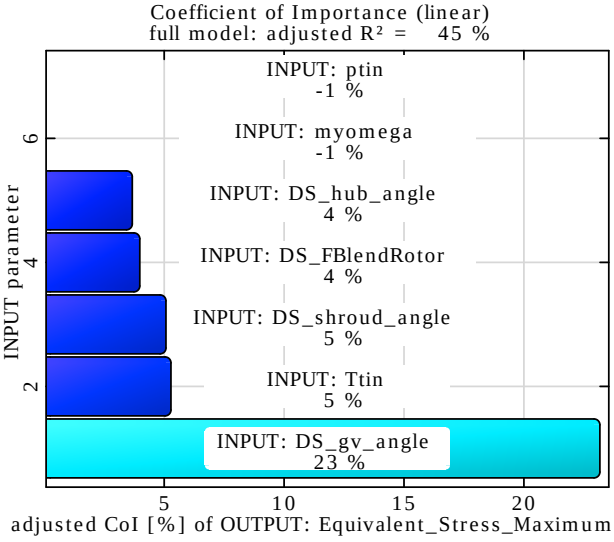

Figure 26: Adjusted value of coefficient of determination R^2_{adj} and coefficients of importance of $\sigma_{\max}$.

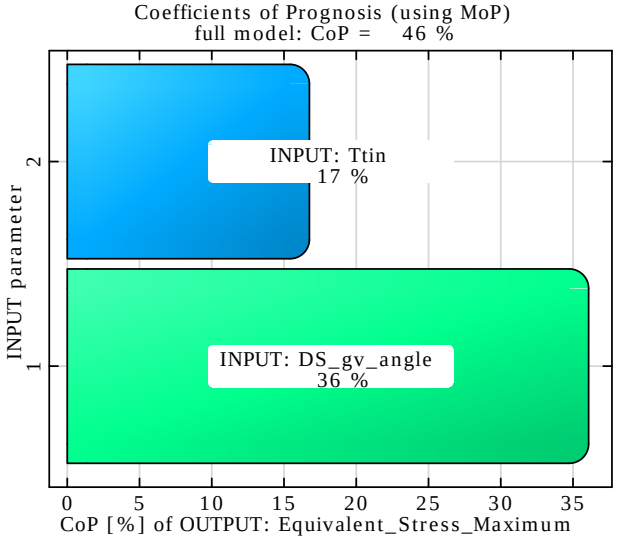

Figure 27: Coefficient of prognosis of $\sigma_{\max}$.

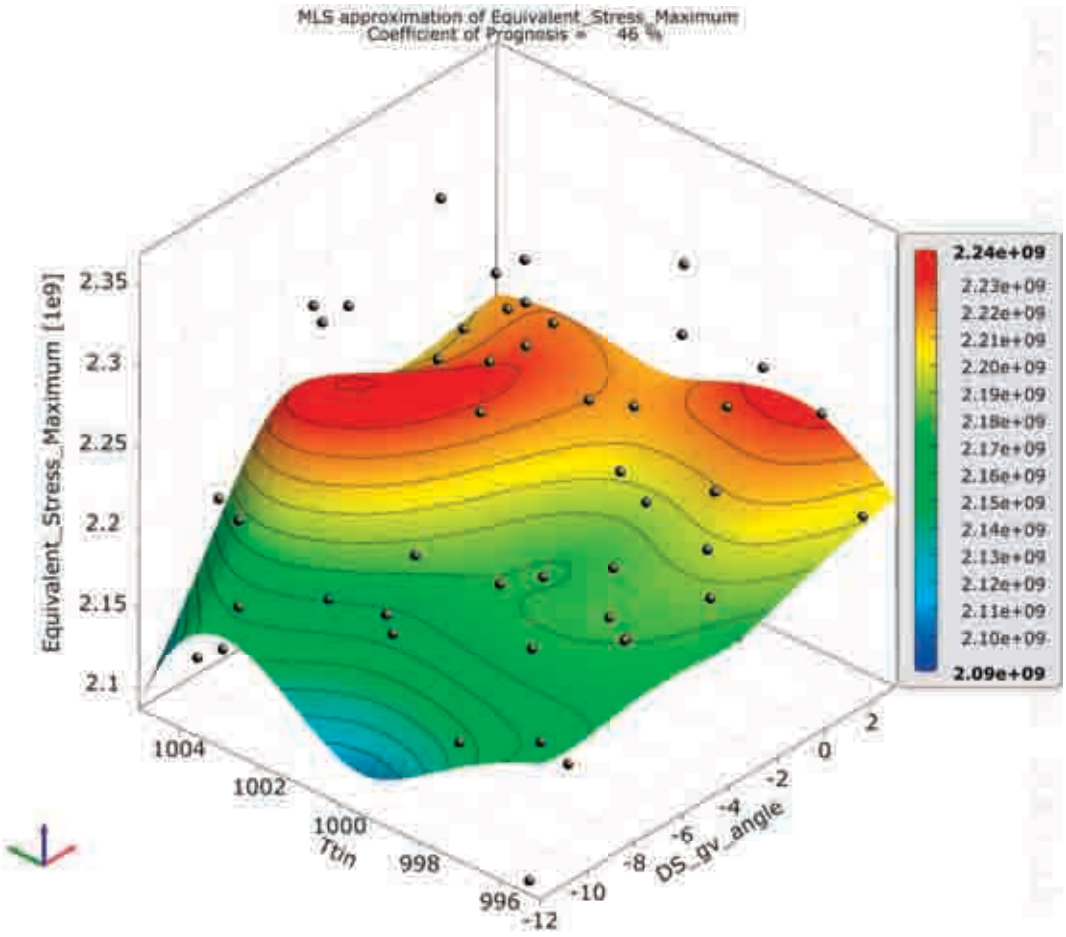

Figure 28: Meta-model of optimal prognosis to approximate $\sigma_{\max}$ in the subspace of the most important input parameters α_{GV} and $T_{t,\mathrm{Inlet}}$.

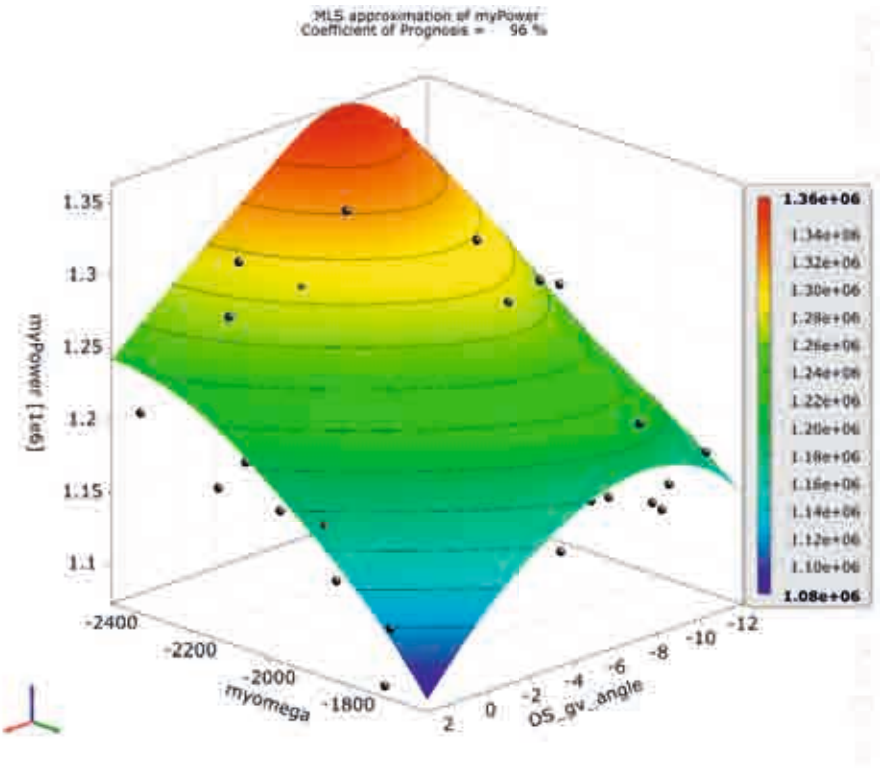

Figure 29: Meta-model of optimal prognosis to approximate the power P in the subspace of the most important input parameters α_{GV} and Ω.

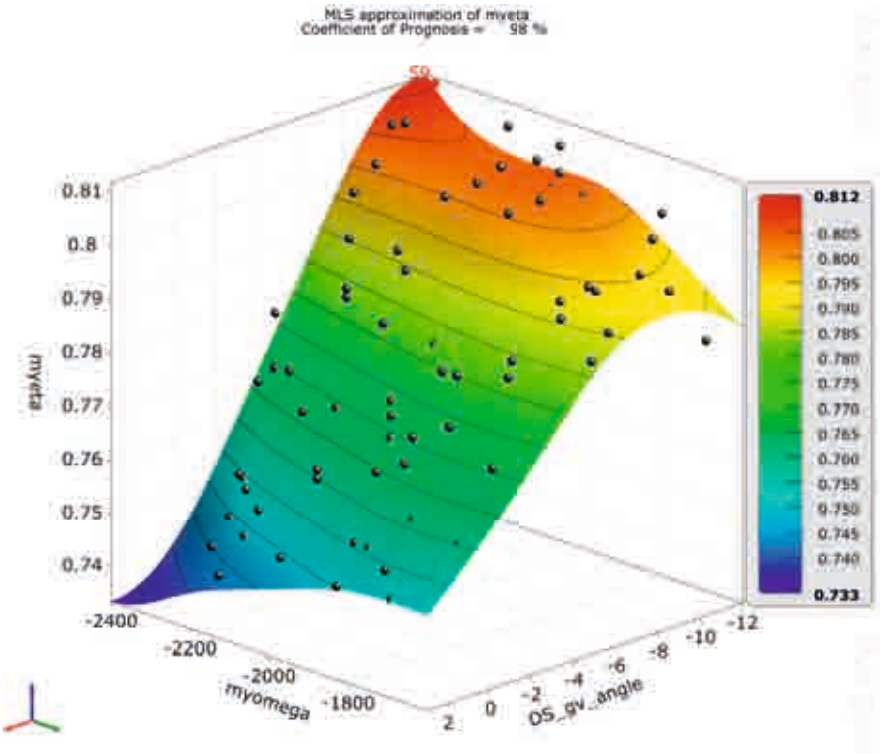

Figure 30: Meta-model of optimal prognosis to approximate the efficiency η in the subspace of the most important input parameters α_{GV} and Ω.

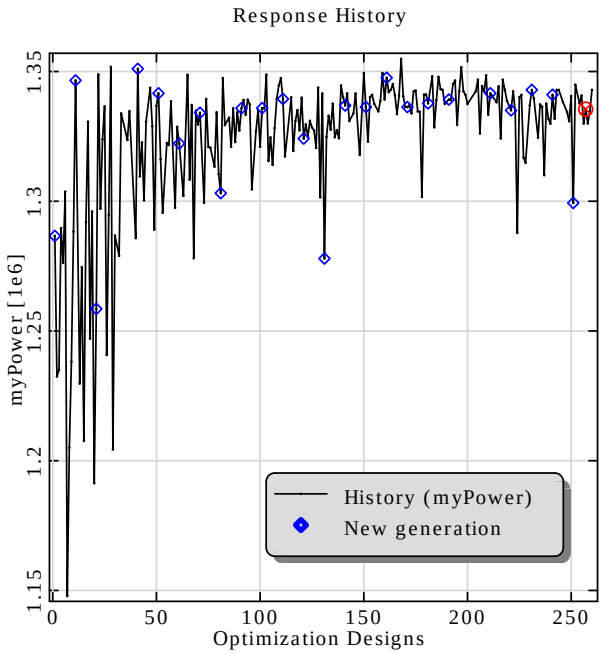

Figure 31: History of the evolutionary algorithm regarding P.

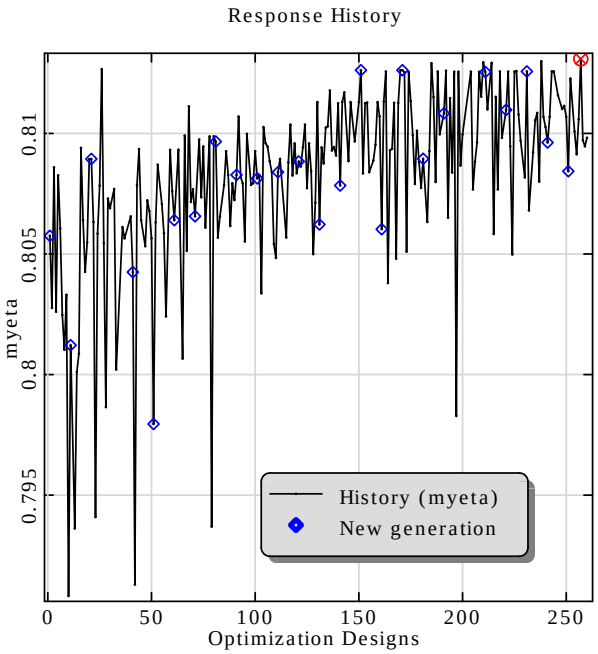

Figure 32: History of the evolutionary algorithm regarding η.

chosen output parameter j, depending on the regression model is the coefficients of importance R^2_{-lj} (see e.g. DYN (2009)). It can be used to detect multivariate significant input parameters l for all response parameters j. All input parameters will have a significant influence to the objective terms, whereby, the importance of the Blade angle of the Hub profile (`DS_hub_angle`) and the Rotor blend radius (`DS_FBlendRotor`) is relatively small with $R^2_{-lj} \leq 0.05$. Therefore, it is not recommended to reduce the number of design parameters for the optimization.

The coefficient of determination of the maximal stress $R^2_{\text{adj}} = 45\%(\leq 80\%)$ is relatively small. Because of that, the result of the Figure 26 should be proven using a meta-model of optimal prognosis including all nonlinearities (see DYN (2009) for detailed reading). For every response parameter the best meta-model is a moving least square approximation using an exponential weighting function, as explained in Roos et al. (2007). The Figures 28 to 30 show these models in the subspace of the input parameters with the two largest coefficients of prognosis, as given in the Figures 23 to 27. In summary, the coefficients of prognosis are similar to the coefficients of importance. Furthermore, the coefficient of prognosis (full model), including all nonlinearities, confirms the coefficient of determination R^2_{adj} of the full linear model. But, as an additional result, the assigned meta-models inform about conflicting objective terms, as shown in Figures 30 and 29 and non-convex restrictions or objectives, as given in Figure 28 and give important knowledge about the choose of the most efficient optimization procedure.

5.6 Global search optimization of the initial design

Unfortunately, as an essential result of the sensitivity analysis, the number of design parameters can not be reduced. All of the input parameters of the Table 2 will have an influence of the objective terms in the Equation (10) and the restriction of the Table 1.

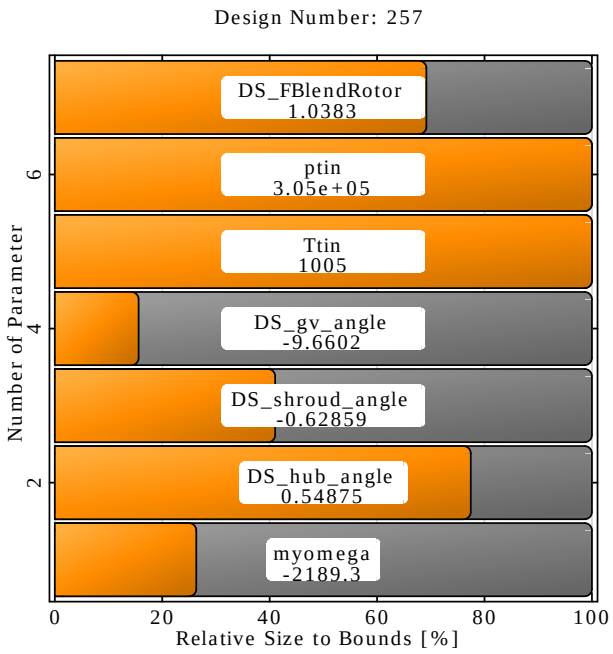

Figure 33: Input parameters of the best design as result of the evolutionary optimization.

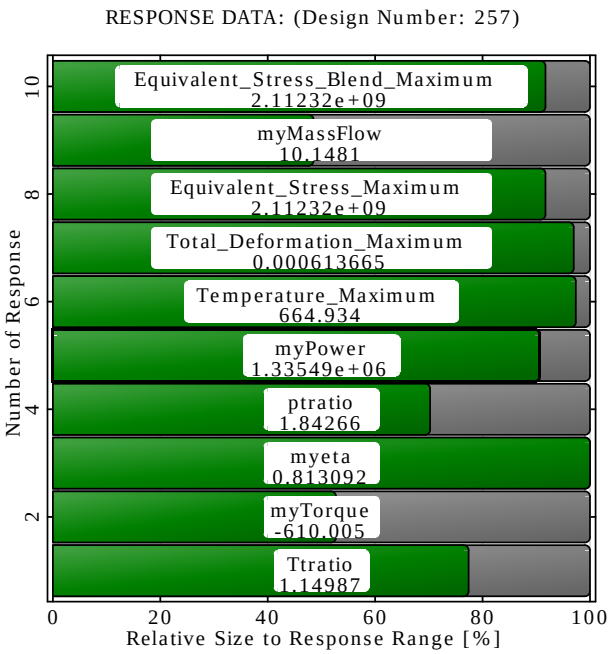

Figure 34: Response parameters of the best design as result of the evolutionary optimization.

Table 4: Responses, restriction and objective of the best design during the design optimization phases. N indicates the number of required design evaluations.

Responses & objective Design phase	Power P	Efficiency η %	Objective function	%	v. Mises stress $\sigma_{\max}$	N
Initial design	$1.2079 \cdot 10^6$	71.645	1.250	100	$2.187 \cdot 10^9$	1
Sensitivity analysis	$1.3413 \cdot 10^6$	80.746	0.887	71	$2.175 \cdot 10^9$	75
Global search optimization	$1.3355 \cdot 10^6$	81.309	0.869	70	$2.112 \cdot 10^9$	198
Local design improvement	$1.3293 \cdot 10^6$	81.544	0.863	69	$2.149 \cdot 10^9$	84

Furthermore, the non-convex stress restriction, as shown in Figure 28 and the conflicting objective terms, as shown in Figures 30 and 29 indicate a global search strategy using an evolutionary algorithm (see DYN (2009) for detailed reading). Figure 20 shows $N = 10$ designs of the latin hypercube sampling procedure which are selected as start population of the first evolutionary optimization step. Based on these start designs the global search strategy converges after $N = 198$ design evaluations. The Figures 31 and 32 explain the convergence history of the power P and efficiency η for all 260 design of experiments (10 start designs, 198 optimization runs, additional 19 identical and 33 unsuccessful design evaluations). The best design #224 (257) with the input parameters is shown in Figure 33 with the associated responses of Figure 34. Because of the very large (concededly random) design improvement of the sensitivity analysis of 29% the improvement of the objective function results in additional 1% only, as collected in Table 4.

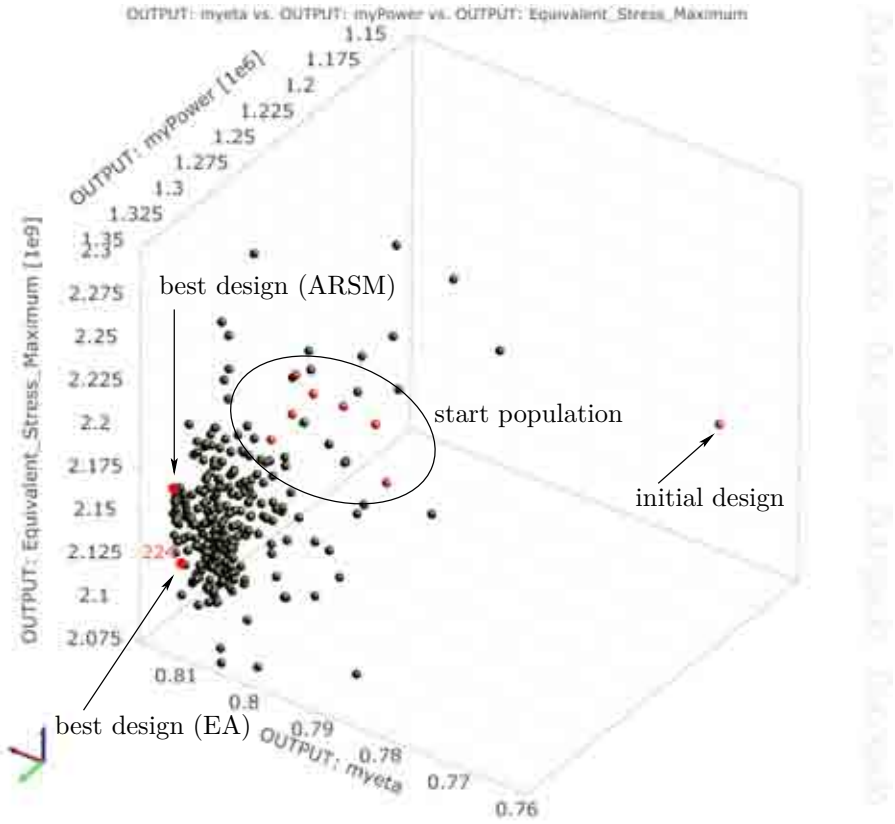

Figure 35: Anthill plot of the 260 design of experiments containing 10 selected start population designs of the sensitivity analysis, 33 unsuccessful and $N = 198$ and additional 19 identical design evaluations of the evolutionary optimization. Furthermore, the responses η, P and $\sigma_{\max}$ of the initial design is shown. The best design of the global search strategy is #224 (257), in comparison with the best design of the adaptive response surface optimization.

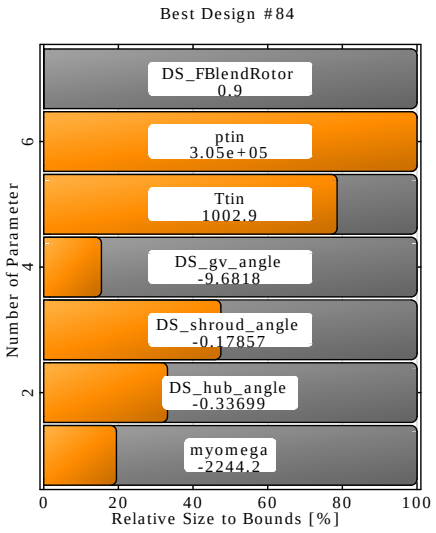

Figure 36: Input parameters of the best design as result of the evolutionary optimization.

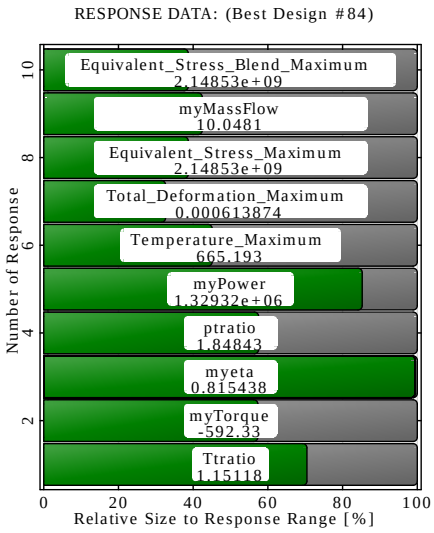

Figure 37: Response parameters of the best design as result of the evolutionary optimization.

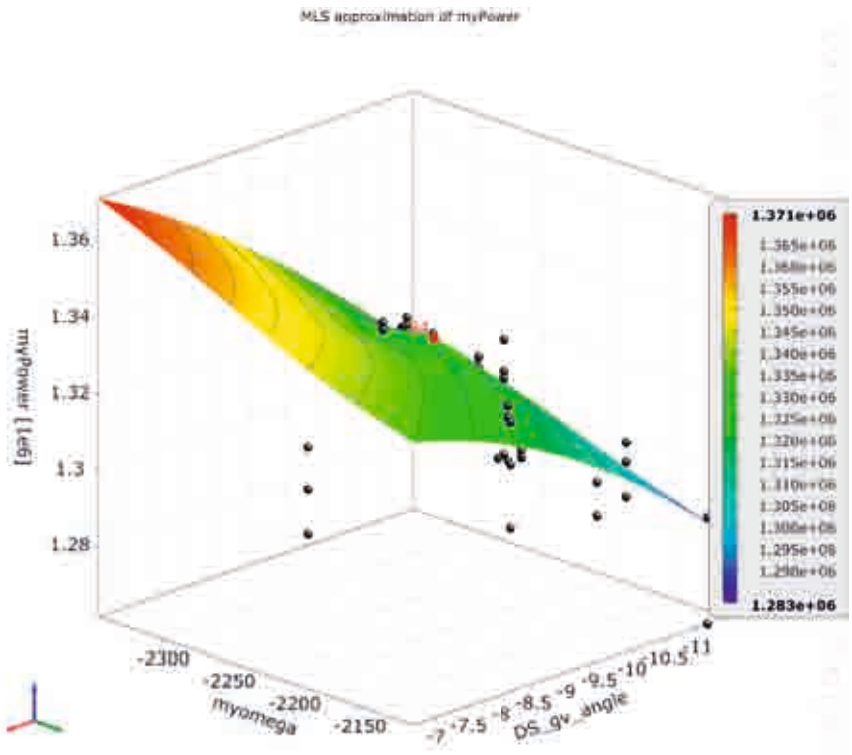

Figure 38: Meta-model and best design #84 of the power P in the subspace of the most important input parameters α_{GV} and Ω.

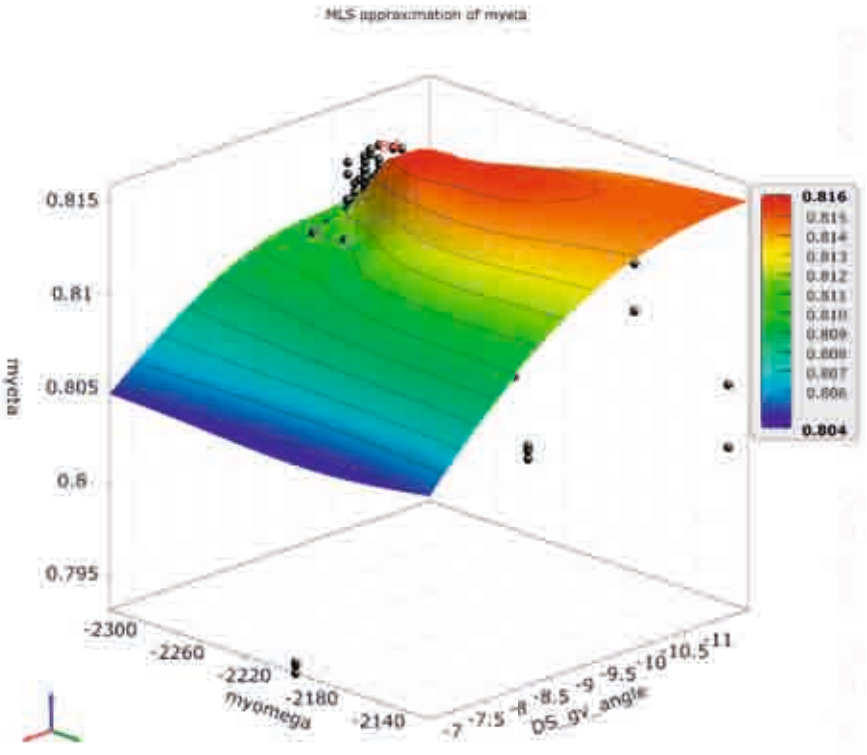

Figure 39: Meta-model and best design #84 of the efficiency η in the subspace of the most important input parameters α_{GV} and Ω.

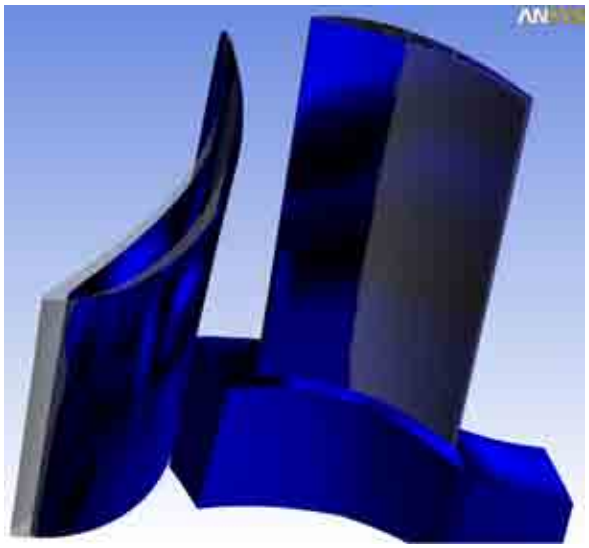

Figure 40: The optimal design with a geometry modification $\alpha_{\text{Hub}} = -0.337$, $\alpha_{\text{Shroud}} = -0.179$ and $\alpha_{\text{GV}} = -9.682$.

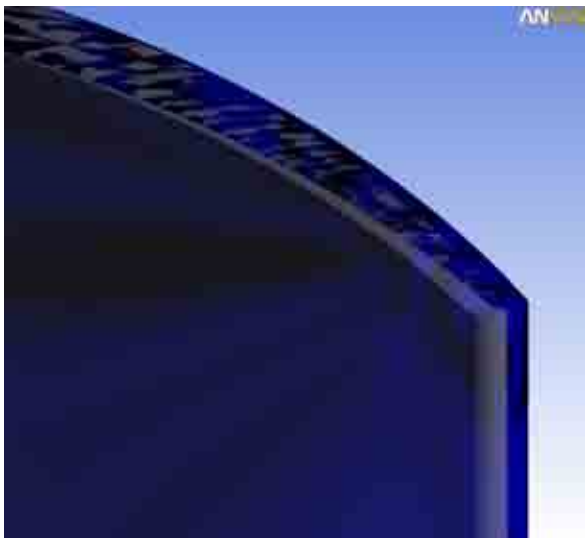

Figure 41: Detail of the modified geometry.

5.7 Design improvement

Subsequent to a global search optimization it is recommended to improve the design using a local optimization strategy. Because of the highly nonlinear structural behavior and possible unsuccessful design evaluations the optimization problem is not continuously differentiable. Therefore, a gradient-free optimization procedure, e.g. an adaptive response surface method is suggested. The adaptive response surface method (see DYN (2009) for detailed reading) does not provide differentiable and smooth problems and is very efficient for $n < 15$ design parameters. The starting solution is based on the best design of the global search optimization and the design space is reduced to 20% around this start solution. The local design improvement converges after $N = 84$ design evaluations with the input parameters are shown in Figure 36 with the associated responses of Figure 37. In summary, the outcome of the deterministic optimization step, as explained in Figure 4, is an increasing of the rotor power P of the turbine engine by 10% and the isentropic efficiency η by 14% compared to the initial design configuration. It follows from the responses a minimization of the objective by 31%, as collected in Table 4, with in total $N = 75 + 198 + 84 = 357$ design evaluations. The optimal design engenders a geometry modification with $\alpha_{\text{Hub}} = -0.337$, $\alpha_{\text{Shroud}} = -0.179$ and $\alpha_{\text{GV}} = -9.682$ as explained in Figures 40 and 41.

5.8 Evaluate the robustness of the optimized design

5.8.1 Global variance-based robustness evaluation

The next step within an iterative stepwise robust design optimization is to evaluate the robustness of the current optimal design. Introducing the given $n_r = 15$ uncertainties of the Table 3 and the manufacturing tolerances an advanced latin hypercube sampling with $N = 47$ design evaluations is used to prove the robustness of the optimized design by means of the target distance of the mean values of the responses to the limit state

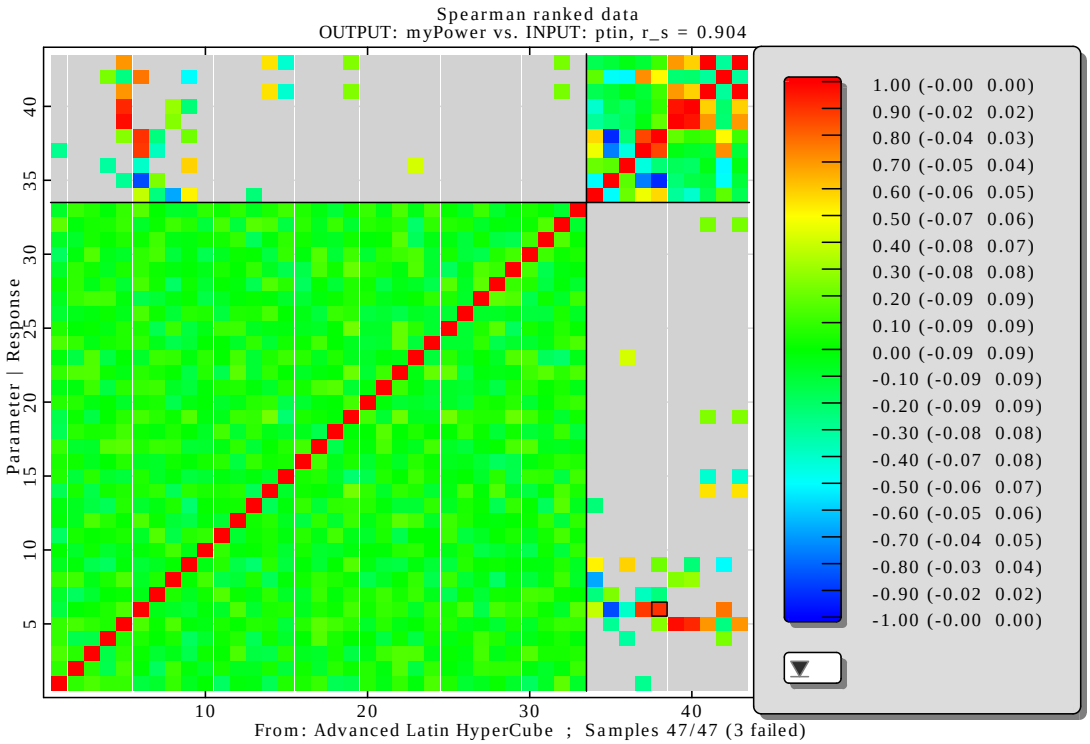

Figure 42: Global variance-based robustness evaluation with $N = 47$ design evaluations and matrix of the linear correlation (including the confidence levels) between random parameters and responses.

conditions in the Table 1. The matrix of the linear coefficients of correlation in Figure 42 shows only few input parameters for each response which have a strong linear correlation. The matrix shows only the statistical significant correlations which are greater than the statistical error of the simulated correlation of the input parameters. The confidence levels of the coefficients of correlation $|\rho_{ij}| = 0.5$ and 0.7 indicate sufficient number of design evaluation.

The Equations (11) and (12) can be used to estimate the safety level. Therefore, in the following we can determine the influence of the random geometry, material, process parameters and the surface uncertainties on the robustness and reliability of the optimized design.

5.8.2 Interpolation of measured imperfections

For the proof of the robustness of the optimized design, manufacturing tolerances are introduced in addition to the randomized operation, geometry and material parameters. The geometry of specimen, either prototypes or parts from the production, can be scanned with stereometric, video or laser based techniques at a high density, as sketched in Fig. 43. By comparison to the CAD reference geometry, statistics of geometry deviations can be obtained. These form the basis for a random field model of manufacturing tolerances. The random field can be sampled by Monte Carlo methods in the way as outlined in section 3.3, yielding a sample set of imperfect geometries. Hence each sample generated in the scope of robustness or reliability analyses consists of a set of random parameters (as listed in Table 3) and random field amplitudes Y_i, cf. eq. (7). The imperfect blades

Figure 43: Measurement of surface geometries by stereometry, to be compared with CAD geometry. (GOM Gmbh)

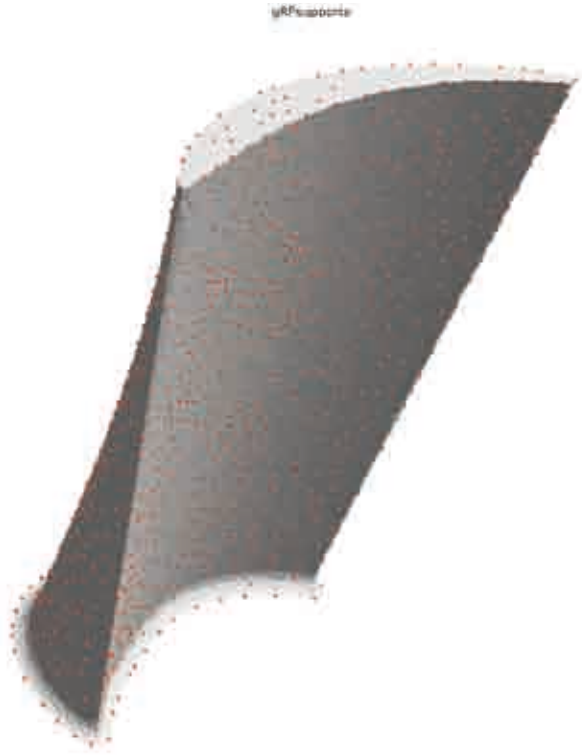

Figure 44: Imperfect geometry of turbine blade is scanned at 1500 points on the surface. A random field is modelled by the statistics of measurements.

generated that way are loaded into the model used for multi-physics computation of the turbine performance.

Due to lack of real data, imperfections were assumed by experience. Geometry deviations are generated in the two directions lateral to the turbine blade. Mean values are constantly zero, standard deviations are inhomogeneous, about 0.01 and 0.0075 mm. The correlations are isotropic with correlation lengths of $L_{XX} = 25mm$.

The geometry is scanned at 1500 points on the surface of the turbine blade, see Fig. 44. The grid of measurement points is usually not compatible with the FE mesh which is used in the analyses. Thus after generating samples of the random field, these have to mapped to the FE mesh. The requirements to the interpolation procedure are: exact fit through the measured values, smooth plot and no artefacts (such as local peaks). The Moving Least Squares interpolation with linear functional basis and regularized weighting (DYN 2009; Most and Bucher 2005) has been evaluated to be the most suitable for this purpose.

5.8.3 Multivariate statistic with uncertainties

An additional result of the global variance-based sensitivity study is the identification of the most significant parameters of the random variables due to important model responses. Figures 45 to 50 show the most significant random parameters out of 15 CAD parameters and 18 random amplitudes which have the largest influence of the variance of the random field. In Figures 45 the adjusted value of coefficient of determination of the full monotone

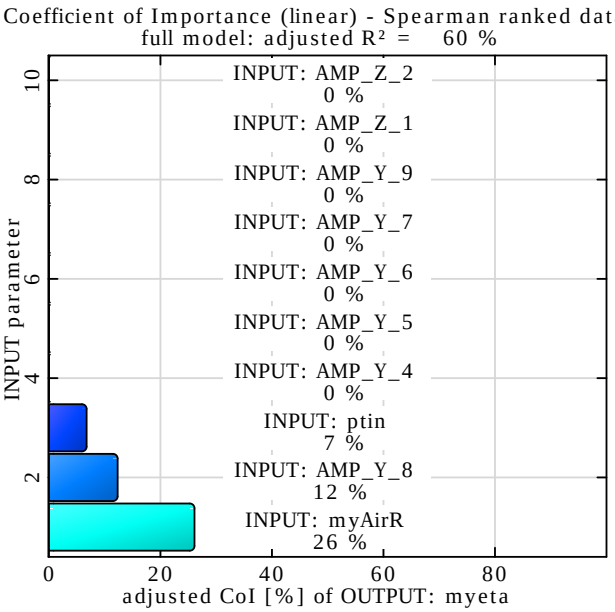

Figure 45: Adjusted value of coefficient of determination R^2_{adj} and coefficients of importance of the efficiency η.

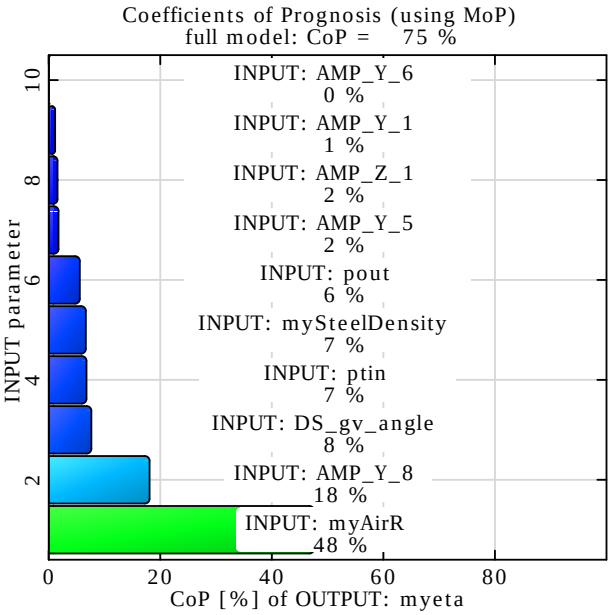

Figure 46: Coefficient of prognosis of the efficiency η.

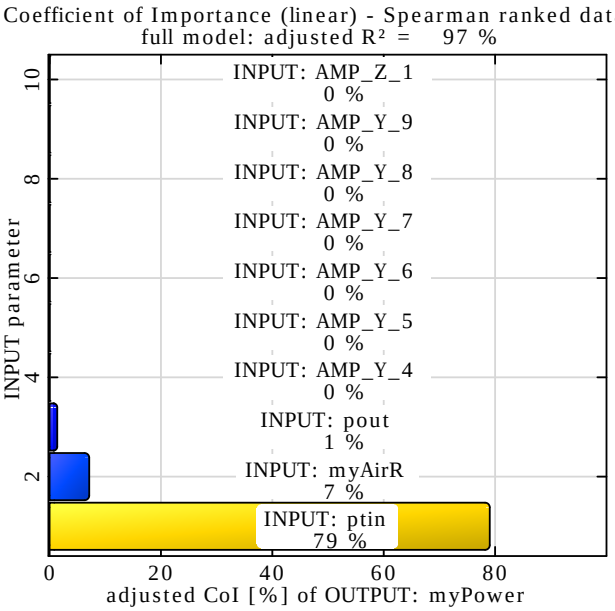

Figure 47: Adjusted value of coefficient of determination R^2_{adj} and coefficients of importance of the power P.

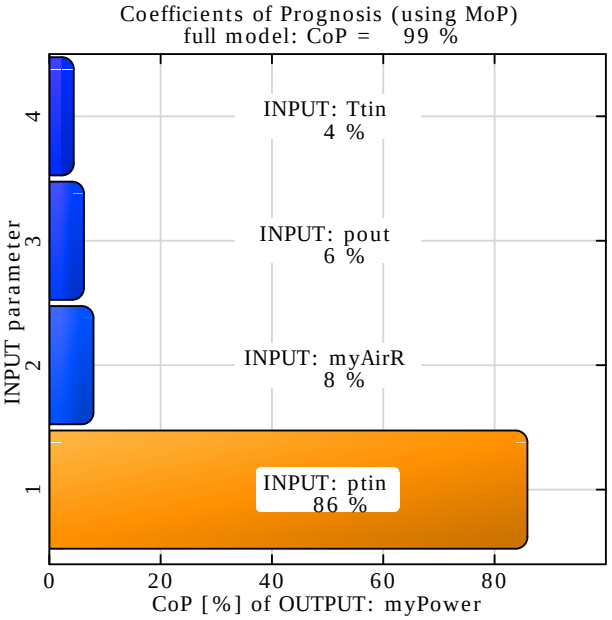

Figure 48: Coefficient of prognosis of the power P.

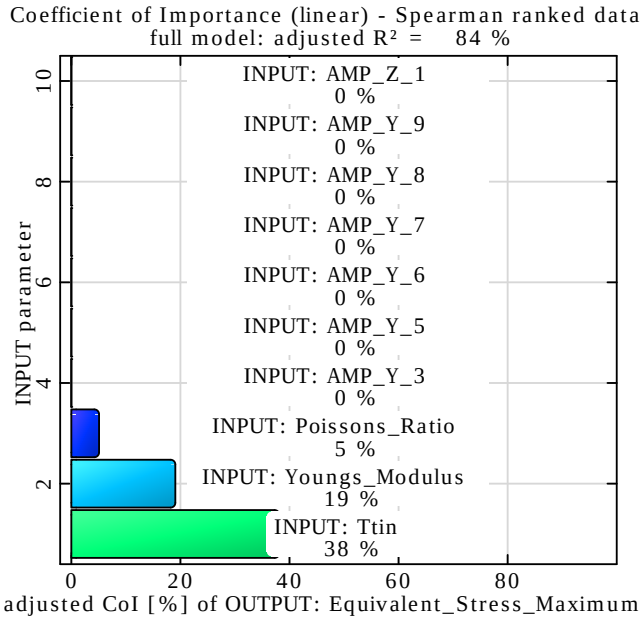

Figure 49: Adjusted value of coefficient of determination R^2_{adj} and coefficients of importance of $\sigma_{\max}$.

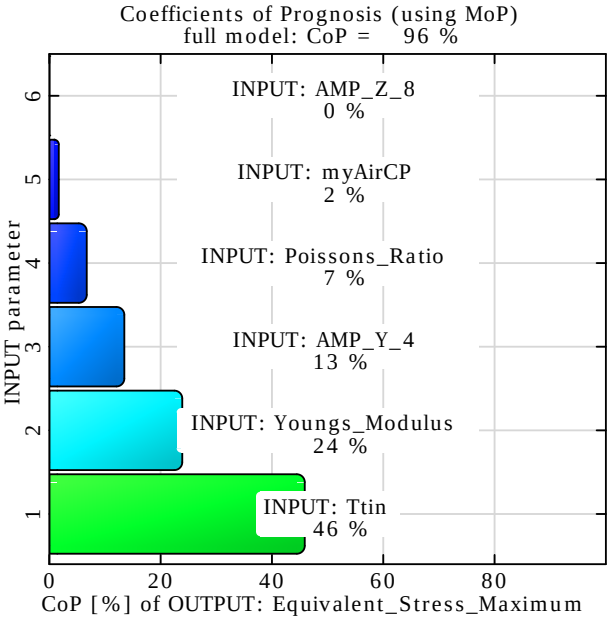

Figure 50: Coefficient of prognosis of $\sigma_{\max}$.

n_r	Description	Name	Symbol	COI	COP
1	Blade angle (Guide vane)	`DS_gv_angle`	α_{GV}	0	8
2	Total temperature inlet	`Ttin`	$T_{t,\text{Inlet}}$	38	46
3	Total pressure inlet	`ptin`	$p_{t,\text{Inlet}}$	79	86
4	Specific gas constant	`myAirR`	R	26	48
5	Density of the steel material	`mySteelDensity`	ρ	0	7
6	Youngs‘ modulus	`Youngs_Modulus`	E	19	24
7	Poissons ratio	`Poissons_Ratio`	ν	5	7
8	Imperfection amplitude	`AMP_Y_4`	$\sigma^2_{Y_4}$	0	13
9	Imperfection amplitude	`AMP_Y_8`	$\sigma^2_{Y_8}$	12	18

Table 5: Identification of the $n_r = 9$ most significant random parameters of the random variables due to important model responses. The prediction values coefficient of importance (COI) and coefficient of prognosis (COP) are taken from the Figures 45 to 50.

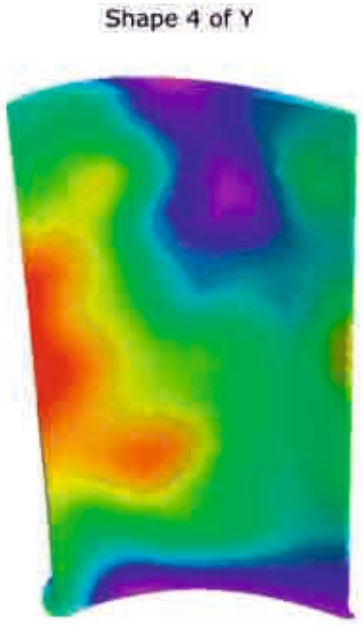

Figure 51: Most significant imperfection amplitude (AMP_Y_4) $\sigma^2_{Y_4}$ of the random field with large influence on $\sigma_{\max}$.

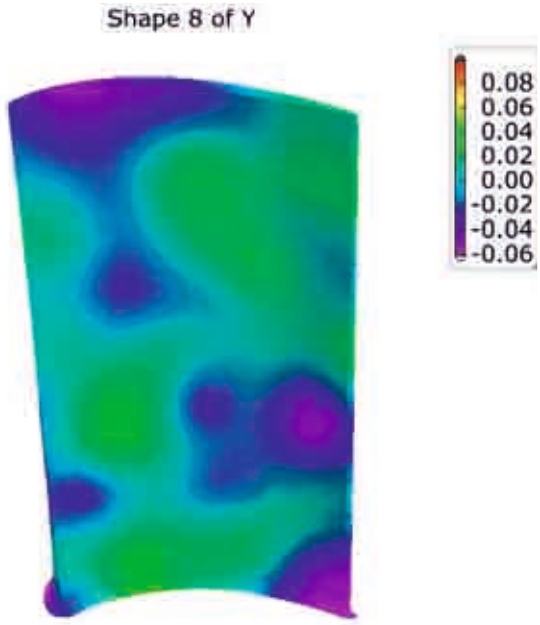

Figure 52: Most significant imperfection amplitude (AMP_Y_8) $\sigma^2_{Y_8}$ of the random field with large influence on η.

nonlinear regression model for the efficiency η is relatively small with $R^2_{\text{adj}} = 60\% < 80\%$. Furthermore,in case of $\sigma_{\max}$, the sum of the single parameter coefficient of importance is not equal to the $R^2_{\text{adj}} = 84\%$. Because of that, the result should be proven using a meta-model of optimal prognosis including all nonlinearities and with respect to possible existing multivariate dependencies. For every response parameter the best meta-model is a moving least square approximation using an exponential weighting function.

The Table 5 puts together these $n_r = 9$ random parameters, which describe the variance of η, P and $\sigma_{\max}$ with 75%, 99% resp. 96% coefficient of prognosis. As an very important result of the robustness evaluation, two imperfection modes with the amplitudes $\sigma^2_{Y_4}$, $\sigma^2_{Y_8}$ (AMP_Y_4,AMP_Y_8) of the random field effect large influences on η and $\sigma_{\max}$, as shown in Figure 51 and 52. We can deduce therefore, that we have to include the influence of the surface uncertainties on the robustness and reliability of the optimized design within a robust design optimization applied to structural, thermal and fluid analysis.

5.9 Reliability analysis of the optimized design

In the previous section the estimation of the failure probability is based on fitting of the histogram with a probability density function using $N = 47$ samples (design evaluations). Figures 53 to 55 show the histograms of power P, efficiency η and the maximal v. Mises stress $\sigma_{\max}$ with the limit state conditions $g_i(\mathbf{x})$ of Table 1.

Of course, the probability levels of the Table 56 are only a rough estimation within a six sigma concept and a reliability analysis of the final design is recommended, especially for small probability levels less than 4.5% or a sigma level greater than 2. With the

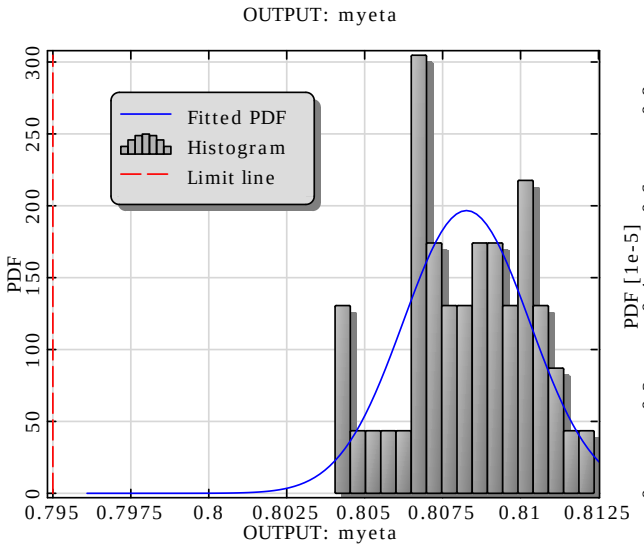

Statistic data			
Min:	0.8041	Max:	0.8124
Mean:	0.8083	Sigma:	0.002028
CV:	0.002509		
Skew ness:	-0.1842	Kurtosis:	2.345
Fitted PDF: Normal			
Mean:	0.8083	Sigma:	0.002028
Limit x = 0.795			
P_rel =	0	P_fit =	3.07755e-11
Probability P(X<x) = 0.95			
x_rel =	0.811073	x_fit =	0.811601

Figure 53: Histogram of η with mean and standard deviation and estimated $P(\mathcal{F}) = 3.1 \cdot 10^{-11}$.

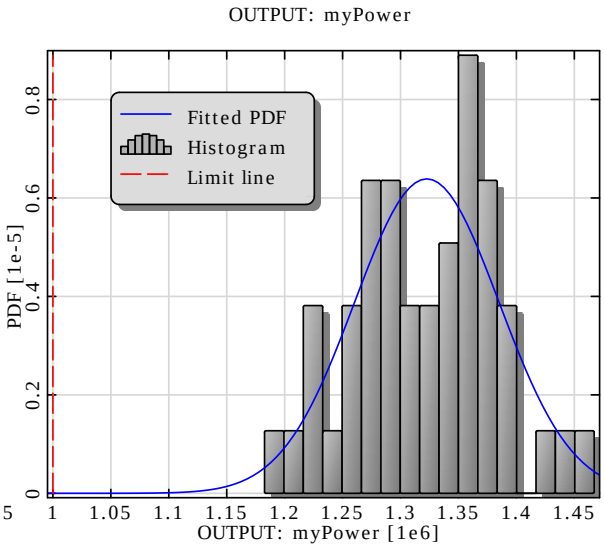

Statistic data			
Min:	1.183e+06	Max:	1.467e+06
Mean:	1.323e+06	Sigma:	6.246e+04
CV:	0.04722		
Skew ness:	-0.03409	Kurtosis:	2.646
Fitted PDF: Normal			
Mean:	1.323e+06	Sigma:	6.246e+04
Limit x = 1e+06			
P_rel =	0	P_fit =	1.19045e-07
Probability P(X<x) = 0.95			
x_rel =	1.43062e+06	x_fit =	1.42543e+06

Figure 54: Histogram of P with mean and standard deviation and estimated $P(\mathcal{F}) = 1.2 \cdot 10^{-07}$.

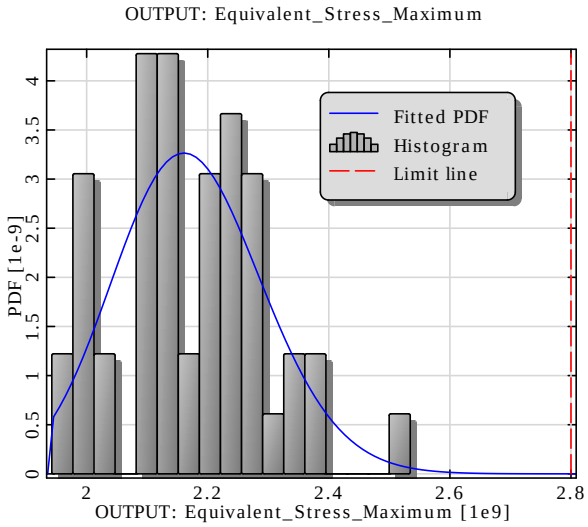

Statistic data			
Min:	1.942e+09	Max:	2.535e+09
Mean:	2.171e+09	Sigma:	1.227e+08
CV:	0.0565		
Skewness:	0.3893	Kurtosis:	3.235
Fitted PDF: Log-Normal			
Mean:	2.171e+09	Sigma:	1.227e+08
Limit x = 2.8e+09			
P_rel =	1	P_fit =	0.999997
Probability P(X<x) = 0.95			
x_rel =	2.37151e+09	x_fit =	2.37861e+09

Figure 55: Histogram of $\sigma_{\max}$ with mean and standard deviation and estimated $P(\mathcal{F}) = 3.0 \cdot 10^{-06}$.

Limit state condition	Sigma level σ_L	$P(\mathcal{F})$ (Equ. 12)	$P(\mathcal{F})$ (PDF)
$g_1(\mathbf{x}, \sigma_{\max})$	5.13σ	$1.45 \cdot 10^{-07}$	$3.0 \cdot 10^{-06}$
$g_2(\mathbf{x}, \eta)$	6.56σ	$2.69 \cdot 10^{-11}$	$3.1 \cdot 10^{-11}$
$g_3(\mathbf{x}, P)$	5.17σ	$1.17 \cdot 10^{-07}$	$1.2 \cdot 10^{-07}$

Figure 56: Sigma levels and associated probability of failure $P(\mathcal{F})$ of the optimized design (assumption: normal distribution of the random response) and estimated $P(\mathcal{F})$ based on the fitted probability density function (PDF).

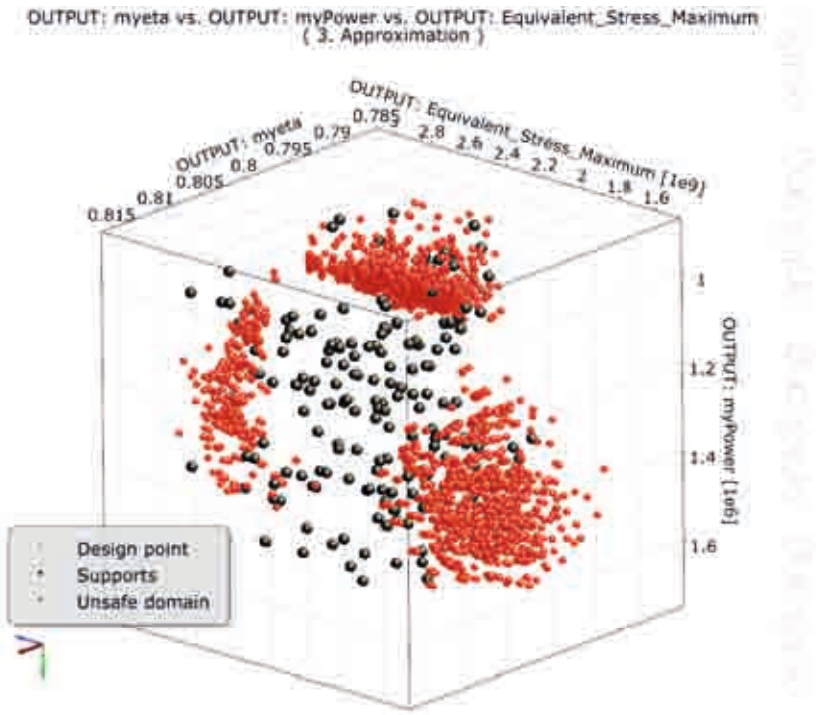

Figure 57: 3D anthill plot of the 174 design evaluations (`Supports`) in the subspace of the responses η, P and $\sigma_{\max}$. The number of clustered areas with high failure probability is equal to the number of limit state conditions. The `Unsafe domain` samples of the directional sampling are used to selected the failure domains.

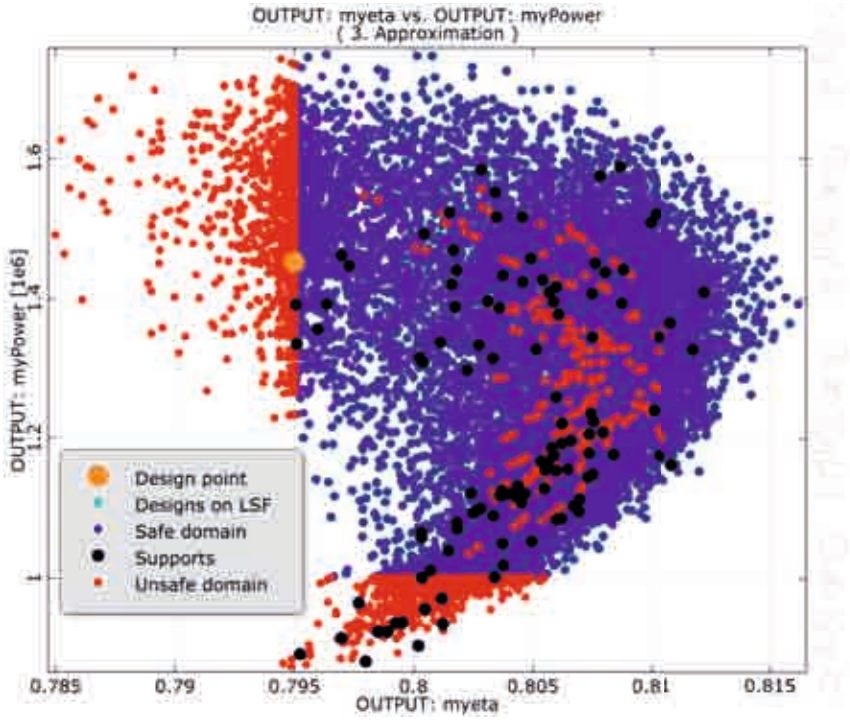

Figure 58: 2D anthill plot of the 174 design evaluations (`Supports`) in the subspace of the responses η and P. The most probable failure point β or `Design point` is located on the limit state function defined by violation of η.

N	Number of designs	174 (6 failed)
Number of samples	Complete directions	10000
	Total	18218
	Safe domain	14356
	Unsafe domain	3862
	Number of clustered areas with high failure probability	3
$P(\mathcal{F})$	Probability of failure	2.556e-07
	Standard deviation error	4.75e-08
Most probable failure point β	DS_gv_angle	-9.45221385684
	Ttin	958.717901531
	ptin	341041.795861
	myAirR	262.501207332
	mySteelDensity	7877.34645619
	Youngs_Modulus	195630092264
	Poissons_Ratio	0.299788054031
	AMP_Y_4	0.00200969530774
	AMP_Y_8	-0.0018453800473
FORM	Distance median - design point (β)	5.674
	Probability of failure	6.972e-09

Table 6: Results and effort of the reliability analysis using directional sampling on adaptive response surfaces. β can be used to evaluate partial safety factors and to compare the calculate $P(\mathcal{F})$ with the estimation using the first order reliability method (FORM).

identification of the random sub domain (see Table 5) directional sampling on adaptive moving least square is used for reliability analysis (Roos and Ochsenfahrt 2009). The moving least square approximation is based on $N = 174$ design evaluations of an adaptive D-optimal design of experiment, as shown in Figures 57 and 58. A cluster analysis is used to detect 3 failure domains with high failure probability and rotatable adaptive designs of experiments can be used to improve the approximation accuracy. The directional sampling procedure on the surrogate model detects samples in the unsafe domain. The assigned failure probability $\bar{P}(\mathcal{F}) = 2.6 \cdot 10^{-7} \leq 3.4 \cdot 10^{-6}$ indicates an optimized Six Sigma Design.

6 Summary

Robust design optimization can provide multiple benefits. It permits the identification of those design parameters that are critical for the achievement of a certain performance characteristic. A proper adjustment of the thus identified parameters to hit the target performance is supported. This can significantly reduce product costs. The effect of variations on the product behaviour and performance can be quantified. Moreover, robust design optimization can lead to a deeper understanding of the potential sources of variations. Hence, a minimization of the effect of variations (noise) is made possible, and appropriate steps to desensitize the design to these variations can be determined. Consequently, more robust and affordable product designs can be achieved.

For the presented variance and probability-based robust design optimization of the

axial turbine the resulting system failure probability could be reduced to a six sigma quality. The process integration of the complex structural, thermal and fluid analysis is based on a parametric workflow management and automatic and embedded solution procedure using the ANSYS Workbench environment with parallel and distributed solver runs using optiSLang .

The robust design optimization respects 7 design parameters and 15 random geometry parameters and additional manufacturing tolerances based on measurements and random field modeling. The presented approach is an iterative decoupled loop in combination with identification of the most significant random and design variables using the multivariate statistic. As a first step the robustness evaluation can be used to prove the predictive capability of the simulation model and to identify the most important parameters and to solve reliability analysis, efficiently.

We can deduce therefore, that we have to include the influence of the surface uncertainties on the robustness and reliability of the optimized design within a robust design optimization applied to structural, thermal and fluid analysis.

Additional result of the optimization procedure is a Six Sigma Design without numerical outliers. In summary, $N = 75 + 198 + 84 + 47 + 174 = 578$ parallel finite element calculations are needed with a total calculation time of 48 hours on 8 Xeon 2.66 GHz CPUs. In this sense, the provided successive robust design optimization approach is applicable for Design for Six Sigma Analysis of real world applications with highly efficiency.

References

V. Bayer and D. Roos. Efficient modelling and simulation of random fields. In *6th Int. Probabilistic Workshop*, Darmstadt, 2009.

V. Bayer, D. Roos, and U. Adam. Structural reliability analysis by random field modeling with robustness methods and adaptive response surfaces. In *11th Int. Conf. Civil, Structural and Enviromental Computing*, St. Julians, Malta, 2007. Civil Comp Ltd.

Aharon Ben-Tal and Arkadi Nemirovski. Robust optimization – methodology and applications. *Mathematical Programming (Series B)*, 92:453 – 480, 2002.

C. E. Brenner. *Ein Beitrag zur Zuverlässigkeitsanalyse von Strukturen unter Berücksichtigung von Systemuntersuchungen mit Hilfe der Methode der Stochastischen Finite Elemente.* Thesis (Dr. tech.). Leopold Franzens Universität Innsbruck, Innsbruck, 1995.

C. Bucher. Basic concepts for robustness evaluation using stochastic analysis. In *Proceedings of the EUROMECH Colloquium 482*, London, September 10-12 2007.

D.M. Byrne and S. Taguchi. The taguchi approach to parameter design. In *40th Annual Quality Congress Transactions*, pages 19 – 26. American Society for Quality Control, Milwaukee, Wisconsin, 1987.

W. Chen, H. Liu, J. Sheng, and H. C. Gea. Application of the sequential optimization and reliabilty assessment method to structural design problems. In *Proceedings of DETC'03, ASME 2003 Design Engineering Technical Conferences and Computers and Information in Engineering Conference*, Chicao, Illinois USA, September 2 – 6 2003.

Ioannis Doltsinis and Zhan Kang. Robust design of structures using optimization methods. *Comput. Methods Appl. Mech. Engrg.*, 193:2221 – 2237, 2004.

optiSLang - the optimizing Structural Language, An Users' Manual. DYNARDO GmbH, Weimar, Germany, 3.1.0 edition, 2009.

R. Ghanem and P.D. Spanos. *Stochastic Finite Elements - a Spectral Approach.* Springer, New York, Berlin, 1991.

K.-H. Hwang, K.-W. Lee, and G.-J. Park. Robust optimization of an automobile rearview mirror for vibration reduction. *Structural and Multidisciplinary Optimization*, 21:300–308, 2001.

P. N. Koch, R.-J. Yang, and L. Gu. Design for six sigma through robust optimization. *Structural and Multidisciplinary Optimization*, 26:235 – 248, 2004.

T. Most and C. G. Bucher. A moving least squares weighting function for the element-free galerkin method which almost fulfills essential boundary conditions. *Structural Engineering and Mechanics*, 21(3):315 – 332, 2005.

A. Papoulis. Probability, random variables, and stochastic processes. In *3rd. edition.* McGraw - Hill, New York, USA, 1991.

M.S. Phadke. *Quality Engineering using Robust Design*. Prentice Hall, Englewood Cliffs, New Jersey, 1989.

D. Roos. Advanced methods of stochastic and optimization in industrial applications. In *Proceedings of the 7th International Conference and Workshop on Numerical Simulation of 3D Sheet Metal Forming Processes, Numisheet*, Interlaken,Switzerland, September 1-5 2008.

D. Roos and D. Ochsenfahrt. Multi-domain adaptive surrogate models for reliability analysis. In *Proceedings of the sixth Weimar Optimization and Stochastic Days*. DYNARDO GmbH, Weimar, Germany, October 15-16, 2009.

D. Roos, U. Adam, and V. Bayer. Design reliability analysis. In *24th CAD-FEM USERS' Meeting 2006*. International Congress on FEM Technology with 2006 German ANSYS Conference, Stuttgart, Schwabenlandhalle, Germany, October 26-27, 2006, 2006.

D. Roos, T. Most, J. Unger, and J. Will. Advanced surrogate models within the robustness evaluation. In *Proceedings of the fourth Weimar Optimization and Stochastic Days*. DYNARDO GmbH, Weimar, Germany, November 28-29, 2007, 2007.